CMS

Bose–Einstein correlations of charged hadrons in proton-proton collisions at $\sqrt{s} = 13\,\text{TeV}$

The CMS Collaboration[*]

Abstract

Bose–Einstein correlations of charged hadrons are measured over a broad multiplicity range, from a few particles up to about 250 reconstructed charged hadrons in proton-proton collisions at $\sqrt{s} = 13\,\text{TeV}$. The results are based on data collected using the CMS detector at the LHC during runs with a special low-pileup configuration. Three analysis techniques with different degrees of dependence on simulations are used to remove the non-Bose–Einstein background from the correlation functions. All three methods give consistent results. The measured lengths of homogeneity are studied as functions of particle multiplicity as well as average pair transverse momentum and mass. The results are compared with data from both CMS and ATLAS at $\sqrt{s} = 7\,\text{TeV}$, as well as with theoretical predictions.

[*]See Appendix C for the list of collaboration members

arXiv:1910.08815v2 [hep-ex] 11 Mar 2020

1 Introduction

Bose–Einstein correlations (BECs) are quantum statistical in nature and were used for several decades to probe the size and shape of the particle emitting region in high energy collisions [1, 2]. These techniques are employed to characterize the size of the emission region at the freeze-out stage of the evolving system. Such studies have been performed by the CMS Collaboration at the CERN LHC in proton-proton (pp) collisions at $\sqrt{s} = 0.9$ TeV [3, 4], 2.36 TeV [3], 2.76 TeV [5] and 7 TeV [4, 5]. In these analyses, the one-dimensional (1D) correlations were measured in terms of the invariant relative momentum $q_{\text{inv}}^2 = -q^\mu q_\mu = -(k_1 - k_2)^2 = m_{\text{inv}}^2 - 4m_\pi^2$ where k_i refers to the four-momentum of each particle of the pair. The pion mass (m_π) is assumed for all of the charged particles, since pions constitute the majority of the produced hadrons. Multi-dimensional analyses of the correlation functions in pp, proton–lead (pPb), and lead–lead (PbPb) collisions were performed by CMS [5] to explore the size of the source in different directions. Similar studies were also performed by other experiments [6–16]. This paper uses CMS data at $\sqrt{s} = 13$ TeV to extend the investigation of one dimensional BECs with charged hadrons produced in pp collisions to include both a higher center-of-mass energy and higher charged particle multiplicities (up to 250 particles).

Studies using pp (and later pPb) events with very high charged particle multiplicities led to the observation of "ridge-like" correlations (i.e., near-side ($\Delta\phi \sim 0$) long-range ($|\Delta\eta| > 2$) anisotropic azimuthal correlations) [17–22] associated with collective flow. In nucleus–nucleus collisions, such structures can be parameterized by a Fourier expansion, providing information about the initial collision geometry and its fluctuations. In hydrodynamic models, initial state anisotropies are propagated to the final state via ultrarelativistic inviscid fluid evolution up to the freeze-out stage of the system. Additional measurements employing high multiplicity (HM) events in pp and in pPb collisions at the LHC resulted in evidence of collective behavior [23, 24] even in such small colliding systems. Altogether, these results indicate that events with high multiplicity produced in pp collisions exhibit some properties similar to those in relativistic heavy ion collisions. The origin of such phenomena in small systems is still under debate [25], and BEC studies supply complementary information to shed light onto the origin of the observed similarities.

In pp collisions, dynamical correlations in the kinematic region of interest for BEC studies can also arise from processes such as resonance decays and jets. In particular, for events with a small number of particles, the relative non-BEC contribution is enhanced. On the other hand, events in the high multiplicity range in pp collisions are more likely than events with similar multiplicities in heavy ion collisions to be affected by multi-jets. Therefore, the importance of accurate removal of these background effects is enhanced for the correlations studied in the current investigation. To address this requirement, the analysis is performed with three techniques that differ from each other in their dependence on simulations.

Correlation functions are used to find the 1D radius fit parameter (R_{inv}, also called the length of homogeneity [26]), and the intercept parameter (λ), corresponding to the intensity of the correlation function at $q_{\text{inv}} = 0$. Fitted values of R_{inv} and λ are presented as functions of event multiplicity as well as average pair transverse momentum ($k_T = \frac{1}{2}|\vec{p}_{T,1} + \vec{p}_{T,2}|$) and mass ($m_T = \sqrt{m_\pi^2 + k_T^2}$). The results are also compared to both previous experimental data and to theoretical predictions.

This paper is structured as follows: Sections 2–4 describe the experimental setup, the datasets and Monte Carlo (MC) simulations employed in the analysis, and the event and track selections, respectively. The generation, correction, and fitting procedures for the correlation func-

tions, and the systematic uncertainties in those procedures, are detailed in Sections 5 and 6, respectively. Results are presented in Section 7, including comparisons with results from pp collisions at $\sqrt{s} = 7\,\text{TeV}$ and theoretical predictions, and the summary is given in section 8. Finally, Appendix A gives additional details on the analysis techniques and Appendix B describes the study of an anticorrelation that was previously seen at lower energies [4, 5]. This anticorrelation is also investigated in pp collisions at 13 TeV over the broad multiplicity range covered by this analysis. In particular, the depth of the dip is nonzero for events with high multiplicity. A more detailed discussion is given in an appendix because this topic is outside the main physics thrust of this paper.

2 The CMS detector

The central feature of the CMS detector is a superconducting solenoid of 6 m internal diameter. Within the solenoid volume are a silicon pixel and strip tracker, a lead tungstate crystal electromagnetic calorimeter (ECAL, $|\eta| < 3$), and a brass and scintillator hadron calorimeter (HCAL, $|\eta| < 3$), each composed of a barrel and two endcap sections, where η is the pseudorapidity. In addition to the barrel and endcap detectors, quartz-fiber Cherenkov hadron forward (HF) calorimeters ($3 < |\eta| < 5$) complement the coverage provided by the barrel and endcap detectors on both sides of the interaction point. These HF calorimeters are azimuthally subdivided into $20°$ modular wedges and further segmented to form 0.175×0.175 ($\Delta\eta \times \Delta\phi$) "towers". A muon system located outside the solenoid and embedded in the steel flux-return yoke is used for the reconstruction and identification of muons up to $|\eta| = 2.4$. The silicon tracker measures charged particles within the pseudorapidity range $|\eta| < 2.5$. It consists of 1440 silicon pixel and 15 148 silicon strip detector modules. For nonisolated particles of $1 < p_\text{T} < 10\,\text{GeV}$ and $|\eta| < 1.4$, the track resolutions are typically 1.5% in p_T and 25–90 (45–150) μm in the transverse (longitudinal) impact parameter [27]. The BPTX (Beam Pickup for Timing for the eXperiments) devices are used to trigger the detector readout. They are located around the beam pipe at a distance of 175 m from the IP on either side, and are designed to provide precise information on the LHC bunch structure and timing of the incoming beams. Events of interest are selected using a two-tiered trigger system [28]. The first level (L1), composed of custom hardware processors, uses information from the calorimeters and muon detectors to select events at a rate of around 100 kHz within a time interval of less than 4 μs. The second level, known as the high-level trigger (HLT), consists of a farm of processors running a version of the full event reconstruction software optimized for fast processing, and reduces the event rate to around 1 kHz before data storage. A detailed description of the CMS detector, together with a definition of the coordinate system and kinematic variables, can be found in Ref. [29].

3 Data and simulated samples

This analysis uses pp data at $\sqrt{s} = 13\,\text{TeV}$ collected at the LHC in 2015. The data were taken using a special LHC configuration providing an average of 0.1 interactions per bunch crossing, resulting in a very low probability of simultaneous pp collisions (pileup). The events were selected using minimum-bias (MB) and HM triggers, with samples corresponding to total integrated luminosities ($\mathcal{L}$) of 0.35 and 459 nb^{-1}, respectively. The different luminosities of the MB and HM samples are due to different prescale factors applied to the number of events that pass the selection criteria of the respective triggers.

The MB events are selected using a trigger that requires at least one tower on either side of the HF to have a deposited energy above 1 GeV. This trigger mainly reduces effects from detector

noise, beam backgrounds, and cosmic rays, while maintaining a high efficiency (greater than 99% for reconstructed track multiplicities above 10, as estimated with simulated samples) for events coming from inelastic proton-proton collisions.

To increase the number of HM events, three triggers with different multiplicity thresholds are used. At L1, these triggers require the scalar sum of the transverse energy in the ECAL, HCAL, and HF towers to be larger than 40, 45, or 55 GeV. At the HLT stage, events are selected by requiring track multiplicities larger than 60, 85, or 110, pre-selected by L1 at 40, 45, or 55 GeV, respectively. In the HLT, tracks are reconstructed using pixel detector information. The low pileup configuration is critical in ensuring a high purity of single pp collisions in the HM dataset.

Monte Carlo simulated event samples are generated using PYTHIA 6.426 [30] and PYTHIA 8.208 [31] with tunes Z2* [32, 33] and CUETP8M1 [33], respectively. For events with generated charged particle multiplicity above 95, PYTHIA 8 simulations used the 4C [34] tune. The event generator EPOS 1.99 with the LHC tune (EPOS LHC) [35] is also used, primarily for systematic uncertainty studies. Interactions of longer-lived unstable particles and the detector response is simulated using GEANT4 [36]. The number of simulated events is 10–20 million for MB and 3–6 million for HM.

4 Event and track selections

Events are selected offline by requiring all of the following conditions:

- At least one reconstructed vertex with a distance with respect to the center of the nominal interaction region of less than 15 cm in the longitudinal (along the beam) direction and of less than 0.15 cm transverse to the beam.
- Beam-related background suppression by rejecting events for which less than 25% of all reconstructed tracks pass the high-purity selection as defined in Ref. [27].
- Coincidence of at least one tower with total energy above 3 GeV in both of the HF calorimeters, a criterion that selects primarily nondiffractive events.

Reconstructed tracks are required to have $|\eta| < 2.4$ and $p_T > 0.2$ GeV as well as the following selections:

- $|\sigma(p_T)/p_T| < 0.1$, where $\sigma(p_T)$ is the uncertainty in the p_T measurement.
- $|d_{xy}/\sigma(d_{xy})| < 3.0$ and $|d_z/\sigma(d_z)| < 3.0$, where the transverse (d_{xy}) and longitudinal (d_z) distances are measured with respect to the primary vertex (defined as the one with the highest track multiplicity in the event), while $\sigma(d_{xy})$ and $\sigma(d_z)$ are the uncertainties in the d_{xy} and d_z measurements, respectively.

In addition, each track is required to have at least one valid hit in one of the pixel detector layers in order to reduce the contamination from processes such as electron pairs from photon conversion and tracks from decays of long-lived resonances.

When determining the reconstructed charged particle multiplicity of an event, slightly different track requirements than those listed above are imposed to be consistent with the criteria used by the HLT to determine this event multiplicity. The quantity $N_{\mathrm{trk}}^{\mathrm{offline}}$ includes tracks within $|\eta| < 2.4$ with $p_T > 0.4$ GeV, selected without the requirement on the number of valid pixel detector hits. Variable bin widths are used, from 3 to 10 units of multiplicity, depending on the value of $N_{\mathrm{trk}}^{\mathrm{offline}}$. The corresponding particle level multiplicity, N_{tracks}, is corrected for the acceptance and efficiency, as described below, and is used for comparisons with other experiments.

1 For characterizing the performance of the track reconstruction, the following quantities have
2 been checked using MC simulations: (i) absolute efficiency (track selection and detector accep-
3 tance); (ii) fraction of misreconstructed tracks; (iii) probability of reconstructing multiple tracks
4 from a single primary particle; (iv) fraction of nonprimary reconstructed tracks. The total effi-
5 ciency is almost constant at 80% for the range $1 < p_T < 10$ GeV and is above 50% for all η and
6 p_T ranges investigated. The misreconstructed track rate (i.e., the rate of reconstructed tracks
7 that do not share at least 75% of their hits with any track at the generator level) tends to slightly
8 increase in the lower ($\lesssim 1$ GeV) p_T region, but it is always below 1%. A similar p_T dependence is
9 observed for the fraction of nonprimary reconstructed tracks, but the rate is always below 2%.
10 The probability of reconstructing multiple tracks from a single primary particle is of the order
11 of 10^{-3} and is negligible compared to the other quantities. Using these estimates, correction
12 factors for each track in a given (η, p_T) bin are determined [37].

5 Bose–Einstein correlation analysis

5.1 Definitions of signal and background

For each event, the sample containing the BEC signal is formed by pairing all same-sign tracks
(i.e. ++ or −− and denoted "SS") with $|\eta| < 2.4$ and $p_T > 0.2$ GeV. Opposite sign pairs (i.e.
+− and denoted "OS"), within the same $|\eta|$ and p_T ranges, are used by two of the analysis
methods for removing non-BEC contributions to the correlation functions. The distributions
in terms of the relative momentum of the pair q_{inv} are divided into bins of the reconstructed
charged particle multiplicity, $N_{trk}^{offline}$, and of k_T.

Although no particle identification is used, the contamination by particles other than charged
pions is expected to be small, since pions are the dominant hadron species in the sample. For
instance, the ratio of kaons to pions is about 12%, and protons to pions is roughly 6% for 7 TeV
pp collisions [38]; for pp collisions at 13 TeV [39], the ratios are 11–12% and 5–6%, respectively,
depending on the track multiplicity range. The unidentified kaons and protons contaminate
the correlation function mainly in the low-q region, where the BEC effect is stronger (the con-
tribution of nonidentical particle pairs depletes the signal). This contamination may lead to a
reduction of the intercept parameter λ as shown in Fig. 6 of Ref. [5] for pp collisions at 7 TeV,
which compares analyses of the same data using correlation functions generated with pairs
of identical charged pions or pairs of unidentified charged hadrons. In contrast, as also seen
in Fig. 6 in Ref. [5], the BEC radius parameter shows consistent results for the two analyses,
and is therefore not significantly affected by the use of unidentified charged particles instead
of identified pion pairs.

Ideally, the background distribution (reference sample) should contain all the physics effects
that are present in the signal distribution, except for the BECs. This reference sample can be
constructed in several ways, most commonly by mixing tracks from different events, as in this
analysis. The default reference sample (called η-mixing) is constructed by pairing SS tracks
from different events using the same procedure as Refs. [3, 4]. Two events are mixed only if
they have similar reconstructed charged particle multiplicity in each of three pseudorapidity
ranges: $-2.4 < \eta < -0.8$, $-0.8 < \eta < 0.8$, and $0.8 < \eta < 2.4$. For determining this matching
criterion, a weight is assigned to each track of the event, depending on the η range in which it
occurs, and these weights are summed for each event. Then, the events are ordered according
to this sum and the mixing is done by selecting two adjacent events in the ordered list and
pairing each track in one event with all of the tracks in the other one. After being combined in
this way, both events are discarded and not included in other pairings.

After choosing the reference sample, a correlation function is defined as a single ratio (SR) having the signal distribution, i.e., the q_{inv} distribution of pairs from the same event as the numerator, and the reference distribution as the denominator:

$$\text{SR}(q_{inv}) \equiv C_2(q_{inv}) = \left(\frac{\mathcal{N}_{ref}}{\mathcal{N}_{sig}}\right)\left(\frac{dN(q_{inv})_{sig}/dq_{inv}}{dN(q_{inv})_{ref}/dq_{inv}}\right), \tag{1}$$

where $C_2(q_{inv})$ refers to the two-particle correlation defined in Eq. (1) by a SR, $\mathcal{N}_{sig}$ and $\mathcal{N}_{ref}$ correspond to the number of pairs estimated by the value of the integral of the signal and reference distributions, respectively. Refinements of this definition are presented in Section 5.4 and in Appendix A.

5.2 Coulomb interactions and correction

The correlation functions include the effect of the quantum statistics obeyed by the pair of identical particles, but are also sensitive to final-state interactions between the charged hadrons. The Coulomb final-state interaction [40] affects the two-particle relative momentum distribution in different ways for SS or OS pairs, creating a depletion (enhancement) in the low q_{inv} range of the correlation function caused by repulsion (attraction) for SS (OS) pairs. The effect of the mutual Coulomb interaction is incorporated in the factor K, the squared average of the relative wave function Ψ, as $K(q_{inv}) = \int d^3\vec{r}\, f(\vec{r})\,|\Psi(\vec{k},\vec{r})|^2$, where $f(\vec{r})$ is the source intensity of emitted particles, with $\vec{r}$ and $\vec{k}$ representing the pair relative separation and relative momentum, respectively [5]. For point-like sources, $f(\vec{r}) = \delta(\vec{r})$ and the integral gives the Gamow factor, which in the case of SS and OS pairs is given by:

$$G_w^{SS}(\zeta) = |\Psi^{SS}(0)|^2 = \frac{2\pi\zeta}{e^{2\pi\zeta}-1}, \quad G_w^{OS}(\zeta) = |\Psi^{OS}(0)|^2 = \frac{2\pi\zeta}{1-e^{-2\pi\zeta}}, \tag{2}$$

where $\zeta = \alpha m/q_{inv}$ is the Landau parameter, α is the fine-structure constant, and m is the particle mass [41].

In a previous CMS analysis [5], no significant differences in the final results were observed in the case of pions when correcting with the Gamow factor or with the full estimate derived for extended (as opposed to point-like) sources [40, 42–44]. Therefore, in this analysis the corrections for the final state Coulomb interaction are performed using the Gamow factor.

5.3 Fitting the correlation function

Ideally, as in the case of static systems, the two-particle correlation function can be related to the Fourier transform of the emitting source distribution at decoupling. Because of their simplicity, parameterizations of the Gaussian type have been used to relate the source distribution and the measured correlation function. In Ref. [3–5], the Gaussian distribution was studied and yielded fit results much worse than for an exponential function or the Lévy class of parameterizations.

In this analysis, the fits performed to the data correlation functions employ symmetric Lévy stable distributions,

$$C_{2,BE}(q_{inv}) = C[1 + \lambda e^{-(q_{inv}R_{inv})^a}]\,(1 + \epsilon\, q_{inv}), \tag{3}$$

where $C_{2,BE}(q_{inv})$ refers to the two-particle BEC, C is a constant, R_{inv} and λ are the (BEC) radius and intercept parameters, respectively. The exponent a is the Lévy index of stability satisfying the inequality $0 < a \leq 2$. If treated as a free parameter when fitting the correlation functions, this exponent usually returns a number between the value characterizing an exponential function ($a = 1$) and that for a Gaussian distribution ($a = 2$). More details can be found in Ref. [45].

The additional term, linear in q_{inv} (proportional to the constant ϵ), is introduced to account for long-range correlations that may be absent in the reference sample. The fit values for ϵ depend on the multiplicity range: negligible for high multiplicity bins (above 100 tracks), and reaching $\sim 0.2\,\text{GeV}^{-1}$ for low multiplicity bins (below 20 tracks).

The Lévy distribution with a as a free parameter returns the best quality fits, but it is not adopted for extracting the results because it does not allow a direct interpretation of the shape of the source distribution by means of a Fourier transform. Fitting with a pure Gaussian distribution ($a = 2$) returns very poor quality fits for all of the multiplicity and k_{T} bins. Therefore, an exponential form (with a fixed at 1.0) is used for the default fit function. For this parameterization, the functional form for the correlation function, $e^{-q_{\text{inv}} R_{\text{inv}}}$, is the Fourier transform of a source function $\rho(t, \vec{x})$ corresponding to a Cauchy–Lorentz distribution. A Laguerre-extended exponential fit function [46] returns a χ^2/dof of the order of unity (where dof is the number of degrees of freedom) and yields the same R_{inv} values as the simple exponential case, with the caveat that the resulting BEC fits depend on additional parameters from the Laguerre polynomial expansion.

A χ^2 test is used in the fitting procedure. A negative log-likelihood ratio, assuming that the bin content of the signal and that of the reference sample histograms are Poissonian distributions (as implemented in Refs. [47, 48]) returned results consistent with the χ^2 approach.

5.4 Analysis techniques

As discussed in the Introduction, both low and high multiplicity correlation functions in pp collisions are particularly sensitive to the influence of non-BEC effects such as resonance decays and jets. To ensure an accurate accounting of these background contributions, and especially to investigate any variability of the final results, the background removal is performed with three techniques that have different degrees of dependence on simulations. Since two of these methods were used in previous CMS BEC studies [3–5], and are described in detail in Ref. [5], they are only briefly summarized here. Additional details can be found in Appendix A.

For the double-ratio (DR) technique [3–5], the numerator is an SR as in Eq. (1) applied to the data, and the denominator is an SR computed similarly with MC events simulated without BEC effects. In each case, the reference samples for data and simulation are constructed in the same way by considering all charged particles instead of only charged pions in the MC. The DR correlation function is fitted using Eq. (3) to obtain R_{inv} and λ. This procedure reduces any bias due to the construction of the reference sample, with the advantage of directly removing non-BEC effects remaining in the data SR. However, it requires the use of well-tuned MC simulations to describe the overall behavior of the data.

The cluster subtraction (CS) [5] technique uses only SRs from data. Correlation functions for OS pairs are used for parameterizing the contamination from resonances and jet fragmentation (called "cluster contribution"), which are still present in the correlation function [17, 19, 49]. The amount of these contributions that is present in the SS pairs is evaluated by using the same shape found for OS pairs and varying the overall scale to fit the data (details are given in Ref. [5]). To find R_{inv} and λ, the correlation function is fitted with a function combining the cluster and Bose–Einstein contributions, with the latter parameterized using Eq. (3).

The hybrid CS (HCS) method, is similar to a method used for pPb data by the ATLAS experiment [48], has less dependence on MC simulations than the DR method and a smaller number of fit parameters to be adjusted to data than the CS method. In contrast to the CS procedure, which is fully based on the control samples in data, the HCS technique uses MC simulations

for converting the fit parameters from OS single ratios into those for SS.

The first step is to fit the SR constructed using MC simulations separately for SS and OS track pairs using:

$$\Omega(q_{\text{inv}}) = \mathcal{N}\left[1 + B\exp\left(-\left|\frac{q_{\text{inv}}}{\sigma_B}\right|^{\alpha_B}\right)\right],$$ (4)

where B and σ_B are fit parameters used to describe the amplitude and the width of the peak near $q_{\text{inv}} = 0$ and α_B defines the overall shape of the function. For OS pairs, the following regions in q_{inv} are excluded from the fitting process due to the contamination of resonance decays: 0.2–0.3 GeV, 0.4–0.9 GeV, and 0.95–1.2 GeV. In addition, the range $q_{\text{inv}} < 0.1$ GeV is excluded because this region has a large contribution from three-body decays. A Gaussian shape ($\alpha_B = 2$) provides a reasonable overall description of the distributions in $N_{\text{trk}}^{\text{offline}}$ and k_{T} bins. The χ^2/dof values are, in general, not compatible with unity. This is expected because of the distorted shape of the distributions, which are dependent on the MC simulation. Examples of SRs using PYTHIA 6 (Z2* tune) are shown in Fig. 1. Two conversion functions relate the amplitudes and the widths of the fits to SS ($++$ and $--$) to those found for OS ($+-$) MC correlations:

$$\left[(\sigma_B)^{-1}\right]^{(++,--)} = \rho\left[(\sigma_B)^{-1}\right]^{(+-)} + \beta,$$ (5)

$$B^{(++,--)} = \mu(k_{\text{T}})\left[B^{+-}\right]^{\nu(k_{\text{T}})}.$$ (6)

The parameters found when fitting the conversion function for the widths, $\rho = 0.82 \pm 0.04$ and $\beta = 0.077 \pm 0.013$, are independent of k_{T} for the PYTHIA 6 (Z2* tune), whereas the parameters relating the amplitudes, μ and ν, are functions of k_{T}. In Fig. 2, the relations between the fit parameters for different bins in k_{T} and $N_{\text{trk}}^{\text{offline}}$ are shown for MB and HM events (for a given k_{T} range, each point in Fig. 2 represents an $N_{\text{trk}}^{\text{offline}}$ bin).

Similarly, single ratios for OS pairs in data are constructed and fitted with the function given by Eq. (4), yielding the parameters B and σ_B for OS data. The conversion functions based on simulation are used to calculate B and σ_B for SS pairs in data. The resulting estimated background, found using $\Omega(q_{\text{inv}})$ in Eq. (4), is included in Eq. (7) to fit SS data:

$$C_2(q_{\text{inv}}) = \Omega(q_{\text{inv}})C_{2,\text{BE}}(q_{\text{inv}}),$$ (7)

where $C_{2,\text{BE}}(q_{\text{inv}})$ describes the BEC component as in Eq. (3) (with a=1). So, the final fit function has two components: one with fixed parameters to describe non–BEC effects and another with fitted BEC parameters. In Fig. 3, examples of fits using this combined function are shown. The shape of the correlation function is not trivial and cannot be described by a simple function, since it is distorted by many components, such as resonances, jets, etc., and the individual contribution of each of these components is not known. Furthermore, when fitting the correlation function, only statistical uncertainties are considered, which are, in general, smaller than 0.5%, depending on the bin. Therefore, it is expected that fitting with a simple exponential function would not necessarily result in a χ^2/dof near unity.

6 Systematic uncertainties

The following sources of systematic uncertainties are investigated: the bias from the particular choice of reference sample with respect to all other constructed possibilities, the bias from the MC simulation tune adopted in the analysis, the influence of the track selection and relevant corrections, the interference of tracks from pileup collisions, the bias from *z*- and *xy*-vertex
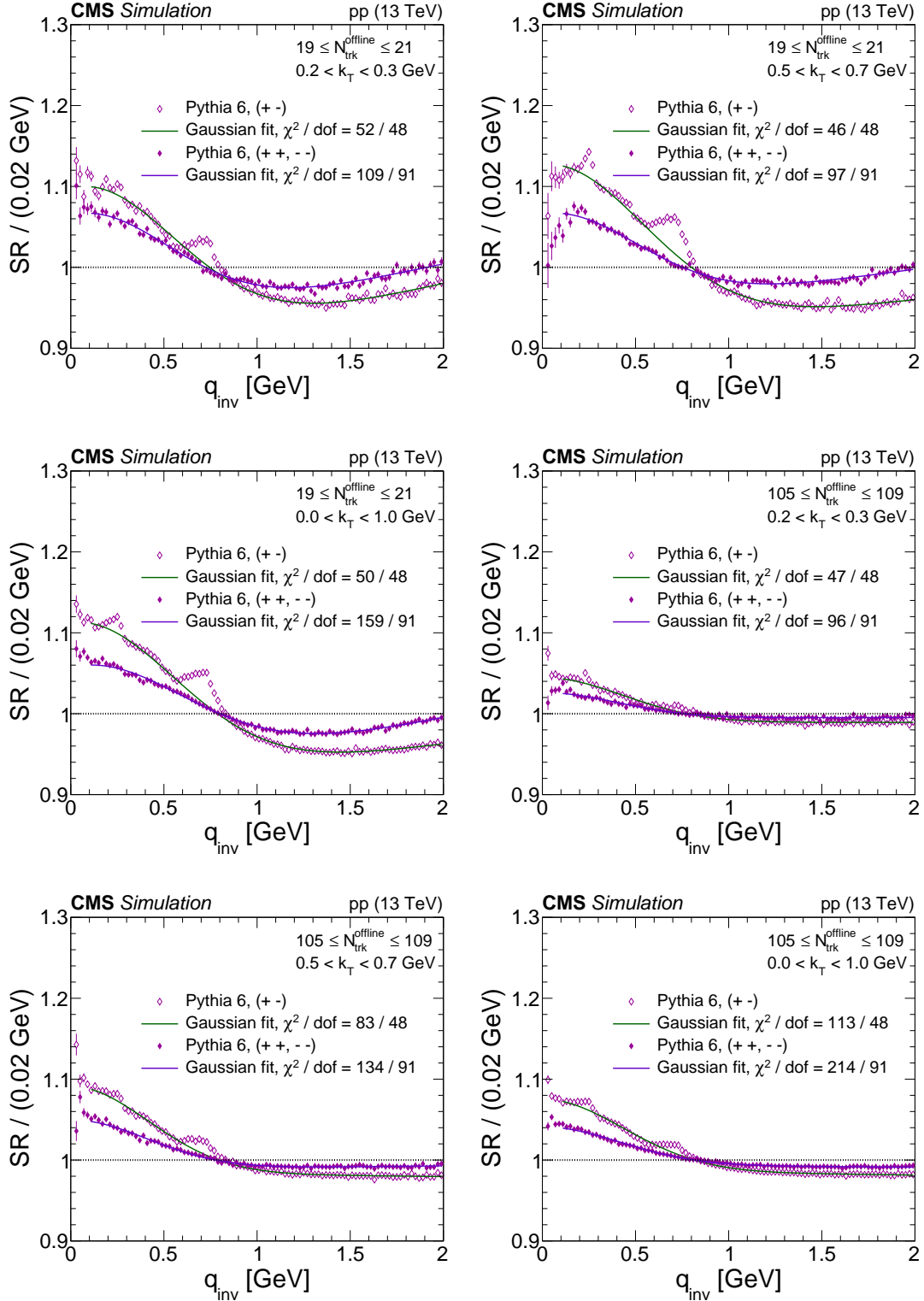
Figure 1: The same-sign $(++, --)$ and opposite-sign $(+-)$ single ratios employing PYTHIA 6 (Z2* tune) in different bins of $N_{\mathrm{trk}}^{\mathrm{offline}}$ and k_{T} with the respective Gaussian fit from Eq. (4). The following q_{inv} ranges are excluded from the fits to the opposite sign single ratios: $0.2 < q_{\mathrm{inv}} <$ 0.3, $0.4 < q_{\mathrm{inv}} < 0.9$, and $0.95 < q_{\mathrm{inv}} < 1.2\,\mathrm{GeV}$. Coulomb interactions are not included in the simulation. The error bars represent statistical uncertainties and in most cases are smaller than the marker size.
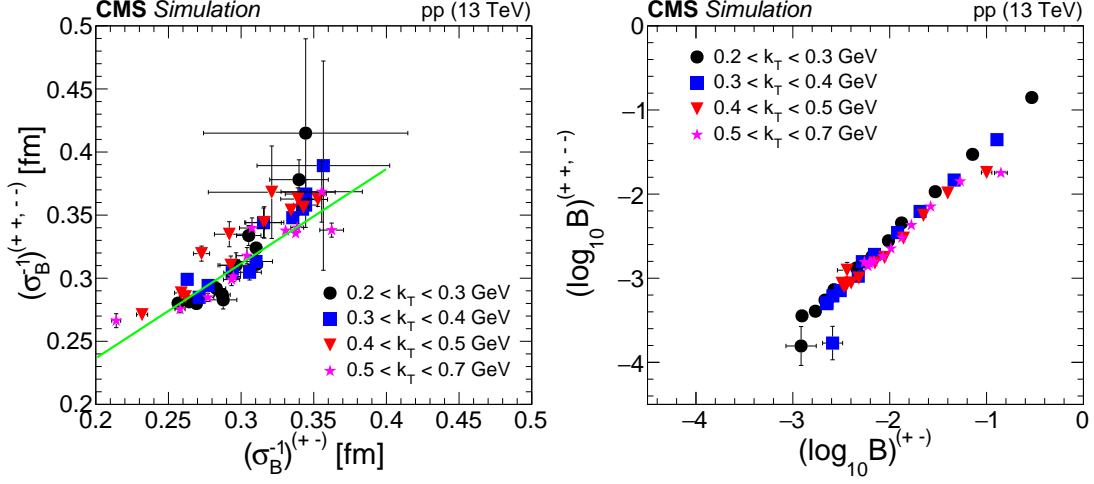
Figure 2: Relations between same-sign $(++, --)$ and opposite-sign $(+-)$ fit parameters from Eq. (4), as a function of k_T and $N_{trk}^{offline}$ for events in MB (i.e., higher σ_B^{-1} and lower $\log_{10}B$) and HM (i.e., lower σ_B^{-1} and higher $\log_{10}B$) ranges. The fit values found for the parameters corresponding to the peak's width (left) and the amplitude (right) of the same-sign and opposite-sign correlations are shown. For a given k_T range, each point represents an $N_{trk}^{offline}$ bin. The line in the left plot is a linear fit to all the data. The error bars represent statistical uncertainties.

positions, the efficiency of the HM triggers, and the effect from the Coulomb correction. The more important biases are those due to the reference samples and the MC simulations. The track selection lead to a nonnegligible effect, mainly in higher-k_T bins, where larger contamination from jets is expected. In addition, the Coulomb correction has a significant contribution. To compute the systematic uncertainties associated with the nonnegligible effects mentioned above, samples of measurements of R_{inv} and λ are generated by varying the corresponding source of bias in bins of $N_{trk}^{offline}$ and k_T, and the root mean square (RMS) spread of each sample is associated with the systematic uncertainty in that bin. The other potential sources of bias listed above returned maximal deviations of the order of the statistical uncertainties ($\sim$1–5%), and are not included in the estimate of the total systematic uncertainty.

To estimate the systematic uncertainties associated with the construction of the reference sample, additional samples are constructed with alternative techniques. Within the category of mixed events, tracks are randomly combined from samples of 25, 40, or 100 events, all of which are in the same range of $N_{trk}^{offline}$. Reference samples are also constructed with tracks from the same event used to form the signal sample, but making pair combinations such that only one of the two tracks has its three-momentum reflected with respect to the origin, i.e., $(p_x, p_y, p_z) \to (-p_x, -p_y, -p_z)$. Another case corresponds to rotating one of these two tracks by 180 degrees in the plane transverse to the beam, i.e., $(p_x, p_y, p_z) \to (-p_x, -p_y, p_z)$.

The uncertainties related to the reference samples and to the MC samples are estimated by associating these two sources and repeating the measurements eighteen times, (6 reference samples)$\times$ (3 MC samples). For the reference samples, the default η-mixing method and the five reference samples described above are used. For MC simulation, samples are generated using PYTHIA 6 (Z2* tune), PYTHIA 8 (CUETP8M1 tune for MB and 4C tune for HM), and EPOS LHC.

For the track selection, in addition to the default definition in Section 4, five additional different configurations were considered, changing combinations of looser and tighter criteria on the
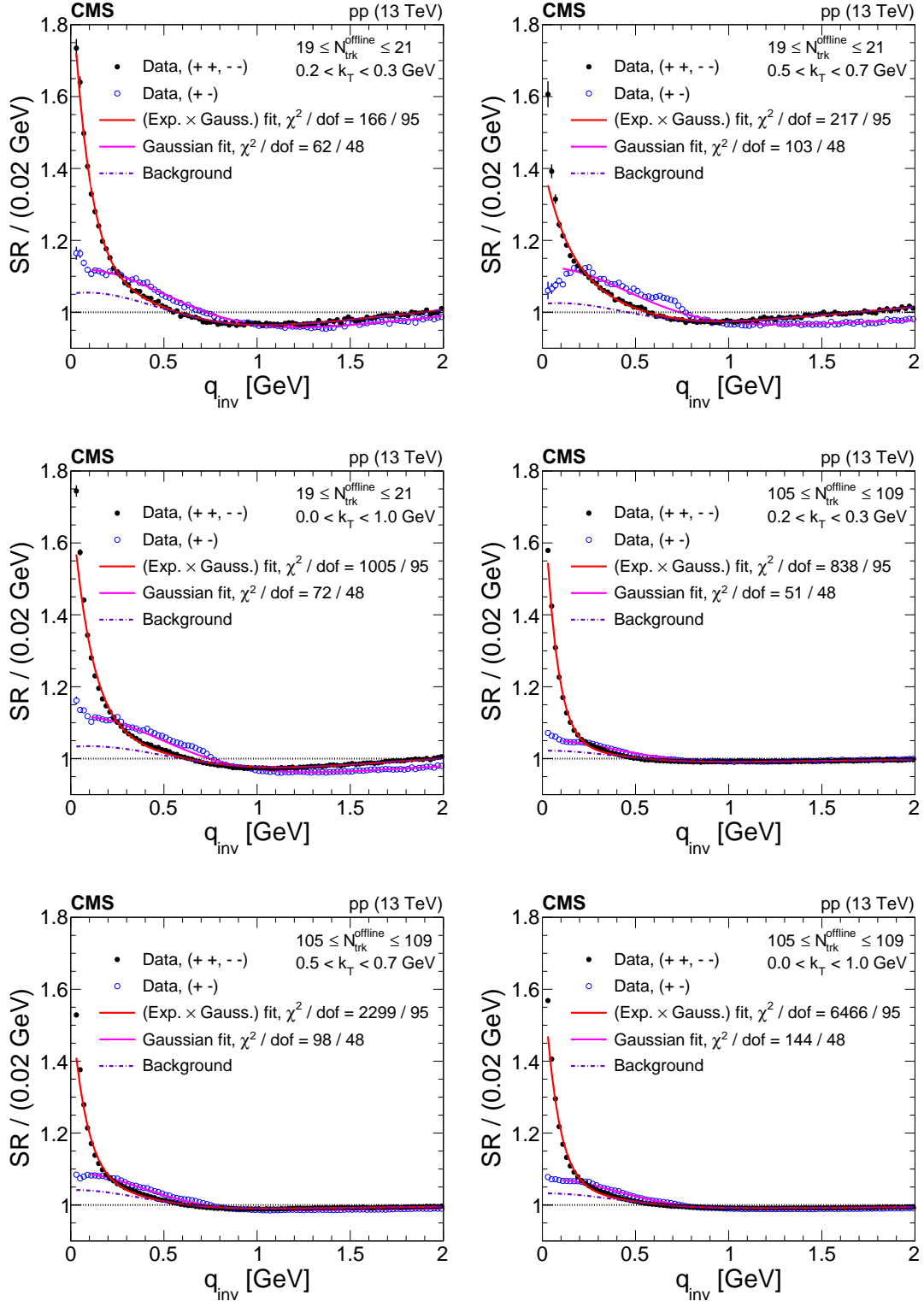
Figure 3: The same-sign $(++, --)$ and opposite-sign $(+-)$ single ratios in data for different bins of $N_{trk}^{offline}$ and k_T, with their respective fits. The label "(Exp. × Gauss.) fit" refers to the same-sign data and is given by Eq. (7). The label "Gaussian fit" corresponds to Eq. (4) applied to opposite-sign data and "Background" is the component of Eq. (7) that is found from the Gaussian fit using Eqs. (5) and (6) to convert the fit parameters. Coulomb corrections are accounted for using the Gamow factor. The error bars represent statistical uncertainties and in most cases are smaller than the marker size.

track variables. These six configurations were used to build a sample of measurements for different track selections.

For the Coulomb correction, a procedure similar to Ref. [3] is adopted, where the Gamow factor is multiplied by a strength parameter κ. Fitting the correlation function by allowing κ to vary yields values consistent with unity within a statistical uncertainty of $\pm15\%$. A conservative uncertainty of 15% applied to the Gamow factor is then propagated, repeating the measurements by varying the magnitude of the Gamow factor up and down by this amount.

Table 1: Total systematic uncertainties in different k_T bins for the hybrid cluster subtraction technique. The ranges in the uncertainties indicate the minimum and maximum values found for all multiplicity bins.

k_T (GeV)	Relative uncertainties	
	$R_{inv}(\%)$	$\lambda(\%)$
Integrated	5–20	5–20
$(0.2, 0.3)$	4–8	5–8
$(0.3, 0.4)$	4–7	4–7
$(0.4, 0.5)$	4–8	4–8
$(0.5, 0.7)$	6–26	9–22

The uncertainties from the three sources listed above are computed independently and then added in quadrature to obtain the total systematic uncertainty. The largest contribution originates from the reference samples and the MC tune, reaching values of $\sim20\%$ in the final measurement. The other sources are always smaller than $\sim6\%$. Table 1 shows the ranges of systematic uncertainties (variation in $N_{trk}^{offline}$) for each k_T bin and integrated in k_T. Lower multiplicities and higher k_T ranges have larger systematic uncertainties because the contamination from the jet fragmentation background is higher in those regions.

7 Results

The values of R_{inv} and λ obtained with each of the three methods as functions of $\langle N_{tracks} \rangle$ and k_T are shown in Fig. 4, where $\langle N_{tracks} \rangle$ is the average multiplicity at particle level corrected for acceptance and efficiency. The top panel presents the results for R_{inv} and λ versus $\langle N_{tracks} \rangle$, for integrated values of the pair transverse momentum in the range $0 < k_T < 1$ GeV. The radius fit parameter R_{inv} increases as a function of multiplicity, showing a change in slope around $\langle N_{tracks} \rangle \sim 20$–30 and a tendency to saturate at higher multiplicities. For the DR and HCS methods, the intercept parameter λ rapidly decreases for increasing multiplicities in the very small $\langle N_{tracks} \rangle$ region, whereas for multiplicities $\gtrsim10$, it shows an almost constant value with increasing $\langle N_{tracks} \rangle$. The systematic uncertainties are larger for λ using the CS method, with the fit values of λ fluctuating and decreasing at higher multiplicities. This happens because λ is very sensitive to the background modeling (non-BEC effects), which leads to larger uncertainties associated with its determination.

In the bottom panel of Fig. 4, fit parameters R_{inv} and λ are shown in two multiplicity bins, MB ($N_{trk}^{offline} < 80$) and HM ($N_{trk}^{offline} \geq 80$), as a function of $\langle k_T \rangle$, where the average is performed in each k_T bin, whose width is variable. The length of homogeneity R_{inv} tends to decrease with increasing k_T, more so at lower multiplicity. This behavior is compatible with an emitting source that was expanding prior to decoupling [26, 50–52]. The correlation intensity λ also decreases with increasing values of k_T, with a more pronounced slope than that for R_{inv}.
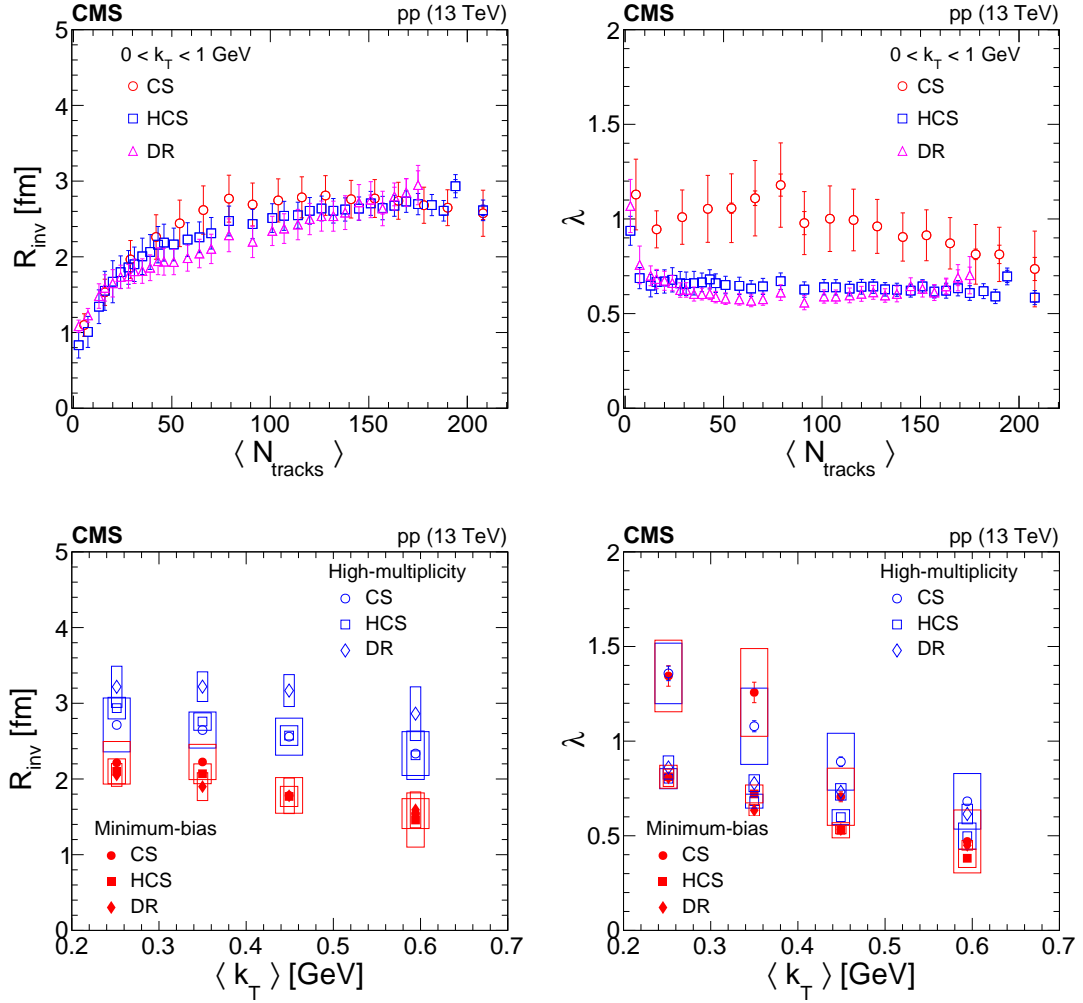
Figure 4: Results for R_{inv} (left) and λ (right) from the three methods as a function of multiplicity (upper) and k_T (lower). In the upper plots, statistical and systematic uncertainties are represented by internal and external error bars, respectively. In the lower plots, statistical and systematic uncertainties are shown as error bars and open boxes, respectively.

The increase of R_{inv} with the event multiplicity and decrease with the average pair momentum in pp collisions were predicted in Ref. [50]. These predictions were based on the assumption that a quark-gluon plasma (QGP) [53–56] could be formed in high energy collisions of small systems in events with multiplicities similar to those investigated here. In the model, high multiplicities are related to large fireball masses formed in the collision, corresponding to a one-dimensional expansion based on Khalatnikov's solution [57] of the Landau hydrodynamical model [58]. These model predictions were also compared to BEC data for pions [6] and kaons [7] measured in pp, $\overline{\text{p}}$p and $\alpha\alpha$ collisions at the CERN ISR, and described the overall behavior of the correlation functions more closely than the Gaussian fit adopted in the analysis of the data.

As shown in Fig. 4, the three methods produce results for R_{inv} that are compatible within the experimental uncertainties. Compatibility tests among the three methods, based on the variations of the measured values, assume the experimental uncertainties are either fully uncorrelated or fully correlated. For the fully correlated, most conservative case, the results agree within two standard deviations for most of the bins investigated. For the CS method, larger deviations are observed for the λ parameter and the associated systematic uncertainties are also larger. This parameter is particularly sensitive to the analysis procedure adopted to remove the non-Bose–Einstein effects present in the signal, as observed in Ref. [5]. Therefore, when comparing to other energies and theoretical models, only the values found using the HCS method are shown. This technique is less sensitive to the MC tune than the DR method, mainly in the HM region, and has smaller systematic uncertainties than the CS method. The ratio of RMS over mean for the differences amongst the values of the radius fit parameters obtained with the three methods is adopted as the relative uncertainty due to the variation between techniques (here called "intramethod variation").

The R_{inv} parameters for pp collisions at 13 TeV are shown in Fig. 5 as a function of multiplicity and compared with the corresponding results obtained in pp collisions at 7 TeV by CMS [5] (left) and ATLAS [15] (right). In the ATLAS measurement, tracks with $p_{\text{T}} > 0.1\,\text{GeV}$ are included in the multiplicity and the correction to particle-level multiplicity is done using an unfolding procedure, as described in Ref. [15]. To have consistent multiplicities, the N_{tracks} values for CMS data in this figure are corrected for the extrapolation down to $p_{\text{T}} = 0.1\,\text{GeV}$. In addition, the opposite-sign $(+-)$ reference sample adopted by ATLAS causes distortions in the same-sign $(++, --)$ correlation functions due to resonance contamination. To circumvent this problem, the ATLAS correlation functions are fitted excluding ranges around the resonance peaks. Therefore, for establishing a more consistent comparison, the analysis with the CMS data was repeated excluding those regions in the fits to both the OS and SS correlation functions. The R_{inv} values for pp collisions at 13 TeV are compatible with those obtained by both CMS and ATLAS at 7 TeV over the entire multiplicity range investigated.

In Fig. 6, the linear dependence of R_{inv} on $N_{\text{tracks}}^{1/3}$ reflects the growth of the number of produced particles with the system volume (or equivalently, $N_{\text{tracks}} \propto R_{\text{inv}}^3$). This dependence is investigated for a range of energies and colliding systems, with the results that, R_{inv} is independent of collision energy when compared at the same multiplicity. Radii can also be studied as a function of $(\text{d}N/\text{d}\eta)^{1/3}$ for investigating the dependence of the final-state geometry on the multiplicity density at freeze-out. Values of R_{inv} are plotted as a function of $\langle N_{\text{tracks}}\rangle^{1/3}$ and $(\text{d}N_{\text{tracks}}/\text{d}\eta)^{1/3}$ in Fig. 6. Statistical uncertainties are represented by the error bars, systematic uncertainties related to the HCS method are shown as the open boxes, and relative uncertainties from the variation between methods are represented by the shaded bands.

Data for R_{inv} and average particle transverse momentum $\langle p_{\text{T}}\rangle$ versus multiplicity were inves-
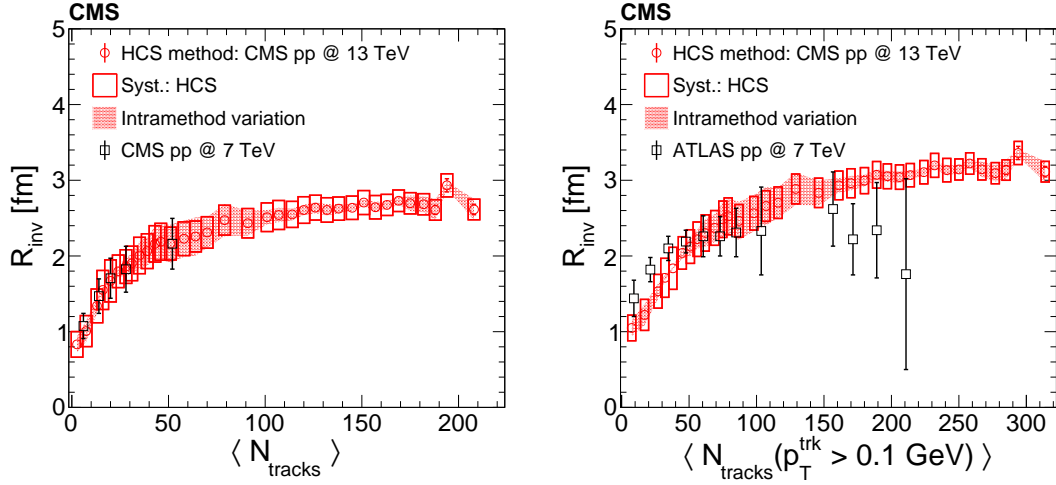
Figure 5: The R_{inv} fit parameters as a function of particle-level multiplicities using the HCS method in pp collisions at 13 TeV compared to results for pp collisions at 7 TeV from CMS (left) and ATLAS (right). Both the ordinate and abscissa for the CMS data in the right plot have been adjusted for compatibility with the ATLAS analysis procedure, as explained in the text. The error bars in the CMS [5] case represent systematic uncertainties (statistical uncertainties are smaller than the marker size) and in the ATLAS [15] case, statistical and systematic uncertainties added in quadrature.

tigated in Ref. [59] to deduce approximate equations of state from experimental measurements in pp and $\overline{\text{p}}$p collisions and search for possible signatures of the phase transition from hadrons to the QGP. A phase transition would cause a change in slope for both observables in the same region of multiplicity per unit pseudorapidity ($dN_{\text{tracks}}/d\eta$). In Ref. [59], the authors claim that their compilation of R_{inv} values as a function of $dN_{\text{tracks}}/d\eta$ for data from several experiments at different center-of-mass energies shows a common behaviour that is independent of the energy. In particular, for R_{inv} obtained by CMS [3] and ALICE [14], they claim that a linear function in $(dN_{\text{tracks}}/d\eta)^{1/3}$ for $dN_{\text{tracks}}/d\eta > 7.5$, matched with a fifth degree polynomial for smaller $dN_{\text{tracks}}/d\eta$ values, fits the data better than a single function of $(dN_{\text{tracks}}/d\eta)^{1/3}$ over the entire range. The $dN_{\text{tracks}}/d\eta$ values in Ref. [59] are for spectra extrapolated to p_{T} of zero and therefore correspond more closely to the right panel of Fig. 5. For the CMS acceptance, a value of $dN_{\text{tracks}}/d\eta \sim 7.5$ corresponds to $\langle N_{\text{tracks}}^{(p_{\text{T}}>0.1)}\rangle \sim 35$ and $\langle N_{\text{tracks}}\rangle \sim 23$. For comparison to Fig. 6, $\langle N_{\text{tracks}}\rangle \sim 23$ is equivalent to $\langle N_{\text{tracks}}\rangle^{1/3} \sim 2.8$ and $\langle dN_{\text{tracks}}/d\eta\rangle^{1/3} \sim 1.7$. This overall qualitative behavior of R_{inv} vs. $\langle N_{\text{tracks}}\rangle$ or $\langle dN_{\text{tracks}}/d\eta\rangle$ seems compatible with the present results shown in Figs. 5 and 6, but the value of R_{inv} around which the data could change slope is not evident, since it is also dependent on the lowest value of p_{T} considered in data.

Although theoretical predictions based on hydrodynamics are not available for pp collisions at 13 TeV yet, expectations for qualitative trends can be found in the literature. A framework based on event-by-event (3+1)-dimensional viscous hydrodynamics, found that the three components of the radius fit parameters continuously grow with $\langle N_{\text{tracks}}\rangle^{1/3}$ for pp collisions [51]. Calculations using a hydrokinetic model also show a linear growth of the lengths of homogeneity with $\langle N_{\text{tracks}}\rangle^{1/3}$ [52]. Such a continuous increase is consistent with the results shown in Fig. 6 and was also observed for different collision systems (CuCu, AuAu, PbPb, and pp) and energies (ranging from 62.4 GeV to 7 TeV) in Fig. 1 of Ref. [51]. To illustrate this expectation from hydrodynamics, a fit with a single linear function over the entire $\langle N_{\text{tracks}}\rangle^{1/3}$ range is shown in the left panel of Fig. 6. A similar trend of increasing length of homogeneity with

multiplicity based on the UrQMD microscopic model for several colliding nuclei at different energies and for pp collisions at 7 TeV is found in Ref. [60]. Instead of the one-dimensional R_{inv} used in the present analysis, which combines temporal and spatial information, Fig. 1 of Ref. [60] shows the three-dimensional radius parameters R_{long} (along the beam) as well as R_{out} and R_{side} (both in the plane transverse to the beam direction), as functions of the charged particle multiplicity at midrapidity, $(\text{d}N_{\text{tracks}}/\text{d}\eta)^{1/3}$. Although the behavior of each radius component varies, a trend of increasing with multiplicity is seen for all colliding systems. In the case of pp collisions, both R_{long} and R_{side} show a clear increasing trend, whereas the R_{out} values estimated by UrQMD show an almost flat behavior or a slight tendency to decrease with increasing multiplicity.

The color glass condensate (CGC) effective theory predicts an increase of the interaction radius (resulting from the initial overlapping of the two protons) as a function of the rapidity density $\text{d}N/\text{d}y$ [61]. This dependence is parametrized by a third order polynomial in terms of $x = (\text{d}N/\text{d}y)^{1/3}$ for $x < 3.4$; beyond this point, the radius tends to a constant value, the so-called "saturation" radius. In the case of pp collisions at 7 TeV, this can be expressed by [61]

$$R_{\text{pp}}(x) = \begin{cases} (1\,\text{fm})[a + bx + cx^2 + dx^3] & (\text{for } x < 3.4) \\ e(\,\text{fm}) & (\text{for } x \geq 3.4) \end{cases} \qquad (8)$$

with parameter values of $a = 0.387$, $b = 0.0335$, $c = 0.274$, $d = -0.0542$, and $e = 1.538$. According to Ref. [61], the minimum multiplicity where the computation in Eq. (8) could be reliable is around $\text{d}N/\text{d}\eta \sim 5$ in cases where no p_{T} cut is applied to the data. This condition is better illustrated by the right plot in Fig. 5, and considering that the η coverage in CMS and ATLAS is about 4.8, this minimum value would correspond to $\langle N_{\text{tracks}}^{(p_{\text{T}}>0.1)} \rangle \sim 25$.
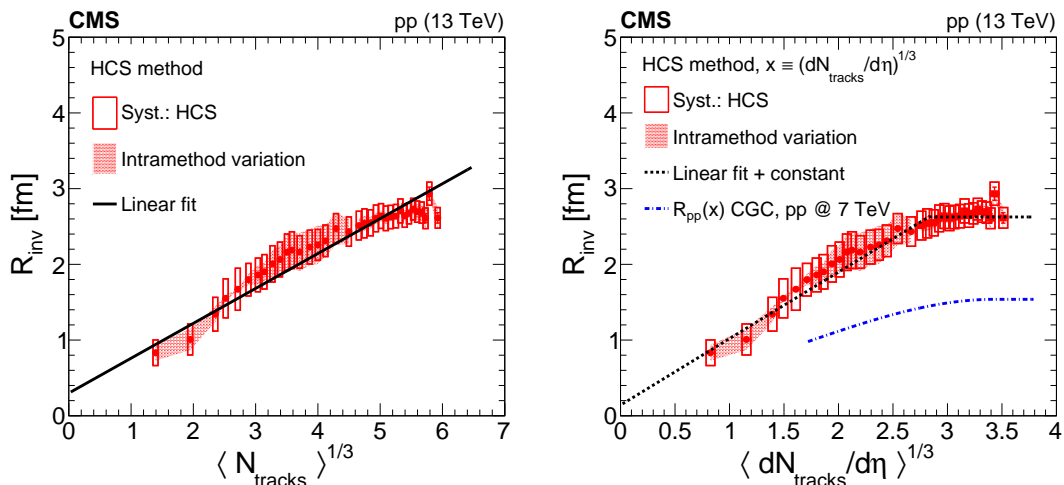

Figure 6: Comparison of R_{inv} obtained with the HCS method with theoretical expectations. Values of R_{inv} as a function of $\langle N_{\text{tracks}} \rangle^{1/3}$ (left) are shown with a linear fit to illustrate the expectation from hydrodynamics. Values of R_{inv} are compared with predictions from the CGC as a function of $\langle \text{d}N_{\text{tracks}}/\text{d}\eta \rangle^{1/3}$ (right). The dot-dashed blue line is the result of the parameterization in Eq. (8). The linear plus constant function (dashed black lines) for $\langle \text{d}N_{\text{tracks}}/\text{d}\eta \rangle^{1/3}$ is shown to illustrate the qualitative behavior suggested by the CGC (the matching point of the two lines is the result of a fit). Only statistical uncertainties are considered.

This prediction for the radius behavior is based on a calculation relating particle multiplicity to a saturation scale using computations of the interaction radius determined from the CGC [62].

The parameterization given in Eq. (8) is compared with the results from the HCS method in the right panel of Fig. 6. The predictions from the CGC are well below the data and the predicted saturation radius [61, 62] is almost half the size of that seen in the data. In Ref. [62], no explicit calculation of the BEC radii (corresponding to emission after the last interaction) is performed. Instead, only the initial size of the pp interaction region and the initial energy density are used, without considering any fluid dynamic evolution, which may explain the underestimated values for the CGC radius parameter seen in Fig. 6. Since the CGC calculation does not include the evolution of the system, it is not unexpected that it underestimates the measured radii. However, the CGC dependence of the radii on particle density, consisting of a rise followed by saturation, is similar to the shape seen in the data. To illustrate this behavior, a linear plus constant function is fitted to the data using statistical uncertainties only (see the right panel of Fig. 6).

The tendency to a constant value of R_{inv} at higher $\langle N_{\mathrm{tracks}} \rangle$ was suggested by ATLAS in Ref. [15], based on their data shown in the right panel of Fig. 5, although their uncertainties were large. In their case, this saturating behavior is considered to be achieved for $\langle N_{\mathrm{tracks}}^{(p_{\mathrm{T}}>0.1)} \rangle \sim 55$, at a much smaller value (less than 1/3) than that suggested by the CGC calculations, where it is claimed that the saturation radius would be reached for $(\mathrm{d}N/\mathrm{d}\eta)^{1/3} \sim 3.4$, or $\langle N_{\mathrm{tracks}} \rangle \sim 190$ charged particles. The new CMS data, with their smaller uncertainties, appear to be more consistent with a saturation at this higher region of multiplicity.
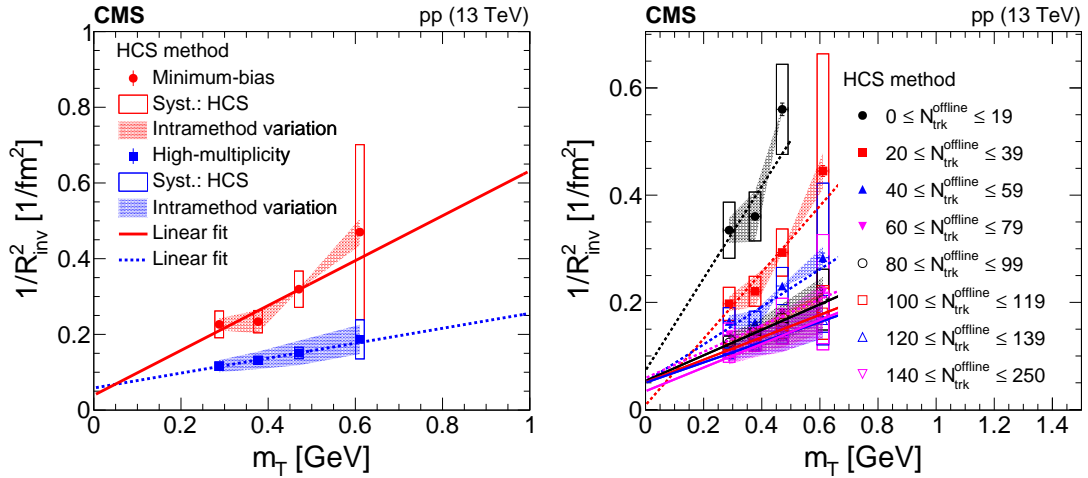
Figure 7: The distribution $1/R_{\mathrm{inv}}^2$ as a function of m_{T} for the HCS method. Results corresponding to the MB range ($0 \leq N_{\mathrm{trk}}^{\mathrm{offline}} \leq 79$) and to the HM one ($80 \leq N_{\mathrm{trk}}^{\mathrm{offline}} \leq 250$) are shown (left). Results are also shown in more differential bins of multiplicity (right). Statistical uncertainties are represented by the error bars, systematic uncertainties related to the HCS method are shown as open boxes, and the relative uncertainties from the intramethods variation are represented by the shaded bands. Only statistical uncertainties are considered in all the fits.

Finally, in hydrodynamic models, valuable information about the collective transverse expansion of the system (transverse flow) can be obtained from the slope of a linear fit to $1/R_{\mathrm{inv}}^2$ versus the transverse mass, m_{T}. In addition, the value of $1/R_{\mathrm{inv}}^2$ at $m_{\mathrm{T}} = 0$ reflects the final-state geometrical size of the source. Figure 7 shows $1/R_{\mathrm{inv}}^2$ versus m_{T} for a variety of multiplicity ranges. The left plot shows that the expansion in the low-multiplicity region is faster than in the HM region. The corresponding geometrical sizes are $R_{\mathrm{G}}^{\mathrm{MB}} = 5.1 \pm 0.4\,(\mathrm{stat})\,\mathrm{fm}$ and $R_{\mathrm{G}}^{\mathrm{HM}} = 4.2 \pm 1.1\,(\mathrm{stat})\,\mathrm{fm}$, for the low and high multiplicity regions, respectively. The right panel of Fig. 7 shows the variations of $1/R_{\mathrm{inv}}^2$ with m_{T} in finer multiplicity ranges, showing in

more detail the evolution of the slope: the collective flow decreases with increasing multiplicity, but this trend seems to saturate around a reconstructed multiplicity of $\sim$80.

This dependence $R_{\mathrm{inv}}^{-2} \propto a + bm_{\mathrm{T}}$ (which was universally observed in nucleus–nucleus collisions, for different colliding system sizes, collision energy, and centrality) implies that the radiiare driven by the initial geometry, as well as by the transverse flow (in a 3D analysis, also by the longitudinal flow). The present data suggest that a similar phenomenological modeling is appropriate for pp collisions at LHC energies. Theoretical models indicate that the intercept of the linear fit to $R_{\mathrm{inv}}^{-2}(m_{\mathrm{T}})$ versus m_{T} equals the geometrical size at freeze-out, whereas the slope gives the square of a Hubble-type flow parameter [63], divided by the freeze-out temperature, i.e., H^2/T_{f} [26, 64]. Assuming $T_{\mathrm{f}} \sim 150\,\mathrm{MeV}$ for the freeze-out temperature, the values of the Hubble-type parameter can be estimated as $H_{\mathrm{HM}} = 0.17 \pm 0.04\,\mathrm{(stat)}\,\mathrm{fm}^{-1}$ and $H_{\mathrm{MB}} = 0.298 \pm 0.004\,\mathrm{(stat)}\,\mathrm{fm}^{-1}$ in the HM and MB regions, respectively.

These values are comparable to those estimated for RHIC AuAu collisions, i.e., $\sim 0.1 - 0.2\,\mathrm{fm}^{-1}$ [12, 65–67], and can also be converted into a flow velocity by multiplying by the measured size. Finally, it should be noted that the extracted Hubble-type parameter is larger in the MB case than in the HM case. These findings are again qualitatively consistent with the measurements in nucleus–nucleus collisions, where the slope parameter of R_{inv}^{-2} vs m_{T} usually shows larger Hubble-type parameters for peripheral than for central collisions. These observations suggest yet another similarity between HM events in high energy pp collisions and relativistic nucleus–nucleus collisions.

8 Summary

A Bose–Einstein correlation measurement is reported using data collected with the CMS detector at the LHC in proton-proton collisions at $\sqrt{s} = 13\,\mathrm{TeV}$, covering a broad range of charged particle multiplicity, from a few particles up to 250 reconstructed charged hadrons. Three analysis methods, each with a different dependence on Monte Carlo simulations, are used to generate correlation functions, which are found to give consistent results. One dimensional studies of the radius fit parameter, R_{inv}, and the intercept parameter, λ, have been carried out for both inclusive events and high multiplicity events selected using a dedicated online trigger. For multiplicities in the range $0 < N_{\mathrm{trk}}^{\mathrm{offline}} < 250$ and average pair transverse momentum $0 < k_{\mathrm{T}} < 1\,\mathrm{GeV}$, values of the radius fit parameter and intercept are in the ranges $0.8 < R_{\mathrm{inv}} < 3.0\,\mathrm{fm}$ and $0.5 < \lambda \lesssim 1.0$, respectively.

Over most of the multiplicity range studied, the value of R_{inv} increases with increasing event multiplicities and is proportional to $\langle N_{\mathrm{tracks}} \rangle^{1/3}$, a trend which is predicted by hydrodynamical calculations. For events with more than $\sim$100 charged particles, the observed dependence of R_{inv} suggests a possible saturation, with the lengths of homogeneity also consistent with a constant value. Comparisons of the multiplicity dependence are made with predictions of the color glass condensate effective theory, by means of a parameterization of the radius of the system formed in pp collisions. The values of the radius parameters in the model are much lower than those in the data, although the general shape of the dependence on multiplicity is similar in both cases. The radius fit parameter R_{inv} is also observed to decrease with increasing k_{T}, a behavior that is consistent with emission from a system that is expanding prior to its decoupling.

Inspired by hydrodynamic models, the dependence of R_{inv}^{-2} on the average pair transverse mass was investigated and the two are observed to be proportional, a behavior similar to that seen in nucleus–nucleus collisions. The proportionality constant between R_{inv}^{-2} and transverse mass can

be related to the flow parameter of a Hubble-type expansion of the system. For pp collisions at 13 TeV, this expansion is slower for larger event multiplicity, a dependence that was also found in nucleus–nucleus collisions. Therefore, the present analysis reveals additional similarities between the systems produced in high multiplicity pp collisions and those found using data for larger initial systems. These results may provide additional constraints on future attempts using hydrodynamical models and/or the color glass condensate framework to explain the entire range of similarities between pp and heavy ion interactions.

Acknowledgments

References

[1] G. Goldhaber, S. Goldhaber, W. Lee and A. Pais, "Influence of Bose-Einstein statistics in the antiproton-proton annihilation process", *Phys. Rev.* **120** (1960) 300, `doi:10.1103/PhysRev.120.300`.

[2] M. A. Lisa, S. Pratt, R. Soltz, and U. Wiedemann, "Femtoscopy in relativistic heavy ion collisions: two decades of progress", *Annu. Rev. Nucl. Part. Sci.* **55** (2005) 357, `doi:10.1146/annurev.nucl.55.090704.151533`, `arXiv:nucl-ex/0505014`.

[3] CMS Collaboration, "First measurement of Bose-Einstein correlations in proton-proton collisions at $\sqrt{s}$ = 0.9 and 2.36 TeV at the LHC", *Phys. Rev. Lett.* **105** (2010) 032001, `doi:10.1103/PhysRevLett.105.032001`, `arXiv:1005.3294`.

[4] CMS Collaboration, "Measurement of Bose-Einstein correlations in pp collisions at $\sqrt{s}$ = 0.9 and 7 TeV", *JHEP* **05** (2011) 029, `doi:10.1007/JHEP05(2011)029`, `arXiv:1101.3518`.

[5] CMS Collaboration, "Bose-Einstein correlations in pp, pPb, and PbPb collisions at $\sqrt{s}$ = 0.9–7 TeV", *Phys. Rev. C* **97** (2018) 064912, `doi:10.1103/PhysRevC.97.064912`, `arXiv:1712.07198`.

[6] AFS Collaboration, "Bose-Esinstein correlations in $\alpha\alpha$, pp and $p\overline{p}$ interactions", *Phys. Lett. B* **129** (1983) 269, `doi:10.1016/0370-2693(83)90859-6`.

[7] AFS Collaboration, "Bose-Einstein correlations between kaons", *Phys. Lett. B* **155** (1985) 128, `doi:10.1016/0370-2693(85)91046-9`.

[8] AFS Collaboration, "Evidence of a directional dependence of Bose-Einstein correlations at the CERN Intersecting Storage Rings", *Phys. Lett. B* **187** (1987) 420, `doi:10.1016/0370-2693(87)91122-1`.

[9] UA1 Collaboration, "Bose-Einstein correlations in $p\overline{p}$ interactions at $\sqrt{s}$ = 0.2 to 0.9 TeV", *Phys. Lett. B* **226** (1989) 410, `doi:10.1016/0370-2693(89)91221-5`.

[10] E735 Collaboration, "Study of the source size in $p\overline{p}$ collisions at 1.8 TeV using pion interferometry", *Phys. Rev. D* **48** (1993) 1931, `doi:10.1103/PhysRevD.48.1931`.

[11] PHOBOS Collaboration, "Transverse momentum and rapidity dependence of HBT correlations in Au+Au collisions at $\sqrt{s_{NN}}$ = 62.4 GeV and 200 GeV", *Phys. Rev. C* **73** (2006) 031901, `doi:10.1103/PhysRevC.73.031901`, `arXiv:nucl-ex/0409001`.

[12] STAR Collaboration, "Pion interferometry in Au+Au collisions at $\sqrt{s_{NN}}$ = 200 GeV", *Phys. Rev. C* **71** (2005) 044906, `doi:10.1103/PhysRevC.71.044906`, `arXiv:nucl-ex/0411036`.

[13] PHENIX Collaboration, "Source breakup dynamics in Au+Au collisions at $\sqrt{s_{NN}}$ = 200 GeV via three-dimensional two-pion source imaging", *Phys. Rev. Lett.* **100** (2008) 232301, `doi:10.1103/PhysRevLett.100.232301`, `arXiv:0712.4372`.

[14] ALICE Collaboration, "Two-pion Bose-Einstein correlations in pp collisions at $\sqrt{s}$ = 900 GeV", *Phys. Rev. D* **82** (2010) 052001, `doi:10.1103/PhysRevD.82.052001`, `arXiv:1007.0516`.

[15] ATLAS Collaboration, "Two-particle Bose-Einstein correlations in pp collisions at $\sqrt{s}$ = 0.9 and 7 TeV with the ATLAS detector", *Eur. Phys. J. C* **75** (2015) 466, `doi:10.1140/epjc/s10052-015-3644-x`, `arXiv:1502.07947`.

[16] LHCb Collaboration, "Bose-Einstein correlations of same-sign charged pions in the forward region in pp collisions at $\sqrt{s}$ = 7 TeV", *JHEP* **12** (2017) 025, `doi:10.1007/JHEP12(2017)025`, `arXiv:1709.01769`.

[17] CMS Collaboration, "Observation of long-range near-side angular correlations in proton-proton collisions at the LHC", *JHEP* **09** (2010) 091, `doi:10.1007/JHEP09(2010)091`, `arXiv:1009.4122`.

[18] ATLAS Collaboration, "Observation of long-range elliptic azimuthal anisotropies in $\sqrt{s}$ = 13 and 2.76 TeV pp collisions with the ATLAS detector", *Phys. Rev. Lett.* **116** (2016) 172301, `doi:10.1103/PhysRevLett.116.172301`, `arXiv:1509.04776`.

[19] CMS Collaboration, "Observation of long-range near-side angular correlations in pPb collisions at the LHC", *Phys. Lett. B* **718** (2013) 795, `doi:10.1016/j.physletb.2012.11.025`, `arXiv:1210.5482`.

[20] ALICE Collaboration, "Long-range angular correlations on the near and away side in p-Pb collisions at $\sqrt{s_{NN}}$ = 5.02 TeV", *Phys. Lett. B* **719** (2013) 29, `doi:10.1016/j.physletb.2013.01.012`, `arXiv:1212.2001`.

[21] ATLAS Collaboration, "Observation of associated near-side and away-side long-range correlations in $\sqrt{s_{NN}}$ = 5.02 TeV proton-lead collisions with the ATLAS detector", *Phys. Rev. Lett.* **110** (2013) 182302, `doi:10.1103/PhysRevLett.110.182302`, `arXiv:1212.5198`.

[22] LHCb Collaboration, "Measurements of long-range near-side angular correlations in $\sqrt{s_{NN}}$ = 5 TeV proton-lead collisions in the forward region", *Phys. Lett. B* **762** (2016) 473, `doi:10.1016/j.physletb.2016.09.064`, `arXiv:1512.00439`.

[23] CMS Collaboration, "Evidence for collectivity in pp collisions at the LHC", *Phys. Lett. B* **765** (2017) 193, `doi:10.1016/j.physletb.2016.12.009`, `arXiv:1606.06198`.

[24] CMS Collaboration, "Measurement of long-range near-side two-particle angular correlations in pp collisions at $\sqrt{s}$ = 13 TeV", *Phys. Rev. Lett.* **116** (2016) 172302, `doi:10.1103/PhysRevLett.116.172302`, `arXiv:1510.03068`.

[25] K. Dusling, W. Li, and B. Schenke, "Novel collective phenomena in high-energy proton-proton and proton-nucleus collisions", *Int. J. Mod. Phys. E* **25** (2016) 1630002, `doi:10.1142/S0218301316300022`, `arXiv:1509.07939`.

[26] A. N. Makhlin and Y. M. Sinyukov, "The hydrodynamics of hadron matter under a pion interferometric microscope", *Z. Phys. C* **39** (1988) 69, `doi:10.1007/BF01560393`.

[27] CMS Collaboration, "Description and performance of track and primary-vertex reconstruction with the CMS tracker", *JINST* **9** (2014) P10009, `doi:10.1088/1748-0221/9/10/P10009`, `arXiv:1405.6569`.

[28] CMS Collaboration, "The CMS trigger system", *JINST* **12** (2017) P01020, `doi:10.1088/1748-0221/12/01/P01020`, `arXiv:1609.02366`.

[29] CMS Collaboration, "The CMS experiment at the CERN LHC", *JINST* **3** (2008) S08004, `doi:10.1088/1748-0221/3/08/S08004`.

[30] T. Sjöstrand, S. Mrenna, and P. Skands, "PYTHIA 6.4 physics and manual", *JHEP* **05** (2006) 026, `doi:10.1088/1126-6708/2006/05/026`, `arXiv:hep-ph/0603175`.

[31] T. Sjöstrand, S. Mrenna, and P. Z. Skands, "A brief introduction to PYTHIA 8.1", *Comput. Phys. Commun.* **178** (2008) 852, `doi:10.1016/j.cpc.2008.01.036`, `arXiv:0710.3820`.

[32] CMS Collaboration, "Study of the underlying event at forward rapidity in pp collisions at $\sqrt{s}$ = 0.9, 2.76, and 7 TeV", *JHEP* **04** (2013) 072, `doi:10.1007/JHEP04(2013)072`, `arXiv:1302.2394`.

[33] CMS Collaboration, "Event generator tunes obtained from underlying event and multiparton scattering measurements", *Eur. Phys. J. C* **76** (2016) 155, `doi:10.1140/epjc/s10052-016-3988-x`, `arXiv:1512.00815`.

[34] R. Corke and T. Sjöstrand, "Interleaved parton showers and tuning prospects", *JHEP* **03** (2011) 032, `doi:10.1007/JHEP03(2011)032`, `arXiv:1011.1759`.

[35] I. Pierog, T. Karpenko, E. Katzy, J. M. Yatsenko, and K. Werner, "EPOS LHC: Test of collective hadronization with data measured at the CERN Large Hadron Collider", *Phys. Rev. C* **92** (2015) 034906, `doi:10.1103/PhysRevC.92.034906`, `arXiv:1306.0121`.

[36] Geant4 Collaboration, "GEANT4—a simulation toolkit", *Nucl. Instrum. Meth. A* **506** (2003) 250, `doi:10.1016/S0168-9002(03)01368-8`.

[37] CMS Collaboration, "Measurement of transverse momentum relative to dijet systems in PbPb and pp collisions at $\sqrt{s_{\mathrm{NN}}}$ = 2.76 TeV", *JHEP* **01** (2016) 006, `doi:10.1007/JHEP01(2016)006`, `arXiv:1509.09029`.

[38] CMS Collaboration, "Study of the inclusive production of charged pions, kaons, and protons in pp collisions at $\sqrt{s}$ = 0.9, 2.76, and 7 TeV", *Eur. Phys. J. C* **72** (2012) 2164, `doi:10.1140/epjc/s10052-012-2164-1`, `arXiv:1207.4724`.

[39] CMS Collaboration, "Measurement of charged pion, kaon, and proton production in proton-proton collisions at $\sqrt{s}$ = 13 TeV", *Phys. Rev. D* **96** (2017) 112003, `doi:10.1103/PhysRevD.96.112003`, `arXiv:1706.10194`.

[40] Y. Sinyukov et al., "Coulomb corrections for interferometry analysis of expanding hadron systems", *Phys. Lett. B* **432** (1998) 248, `doi:10.1016/S0370-2693(98)00653-4`.

[41] M. Gyulassy, S. K. Kaufmann, and L. W. Wilson, "Pion interferometry of nuclear collisions. I. Theory", *Phys. Rev. C* **20** (1979) 2267, `doi:10.1103/PhysRevC.20.2267`.

[42] S. Pratt, "Coherence and Coulomb effects on pion interferometry", *Phys. Rev. D* **33** (1986) 72, `doi:10.1103/PhysRevD.33.72`.

[43] M. Biyajima and T. Mizoguchi, "Coulomb wave function correction to Bose-Einstein correlations", (1994). SULDP-1994-9.

[44] M. G. Bowler, "Coulomb corrections to Bose-Einstein correlations have been greatly exaggerated", *Phys. Lett. B* **270** (1991) 69, `doi:10.1016/0370-2693(91)91541-3`.

[45] T. Csörgő, and S. Hegyi and Zajc, W. A., "Bose-Einstein correlations for Lévy stable source distributions", *Eur. Phys. J. C* **36** (2004) 67, `doi:10.1140/epjc/s2004-01870-9`, `arXiv:nucl-th/0310042`.

[46] T. Csörgő, A. T. Szerzo and S. Hegyi, "Model independent shape analysis of correlations in 1, 2 or 3 dimensions", *Phys. Lett. B* **489** (2000) 15, `doi:10.1016/S0370-2693(00)00935-7`, `arXiv:hep-ph/9912220`.

[47] E802 Collaboration, "System, centrality, and transverse mass dependence of two pion correlation radii in heavy ion collisions at 11.6 A and 14.6 A GeV/c", *Phys. Rev. C* **66** (2002) 054906, `doi:10.1103/PhysRevC.66.054906`, `arXiv:nucl-ex/0204001`.

[48] ATLAS Collaboration, "Femtoscopy with identified charged pions in proton-lead collisions at $\sqrt{s_{NN}}$ = 5.02 TeV with ATLAS", *Phys. Rev. C* **96** (2017) 064908, `doi:10.1103/PhysRevC.96.064908`, `arXiv:1704.01621`.

[49] PHOBOS Collaboration, "System size dependence of cluster properties from two-particle angular correlations in Cu+Cu and Au+Au collisions at $\sqrt{s_{NN}} = 200$ GeV", *Phys. Rev. C* **81** (2010) 024904, `doi:10.1103/PhysRevC.81.024904`, `arXiv:0812.1172`.

[50] Y. Hama and Sandra S. Padula, "Bose-Einstein correlation of particles produced by expanding sources", *Phys. Rev. D* **37** (1988) 3237, `doi:10.1103/PhysRevD.37.3237`.

[51] P. Bozek and W. Broniowski, "Size of the emission source and collectivity in ultra-relativistic p-Pb collisions", *Phys. Lett. B* **720** (2013) 250, `doi:10.1016/j.physletb.2013.02.014`, `arXiv:1301.3314`.

[52] V. M. Shapoval, P. Braun-Munzinger, I. A. Karpenko, and Yu. M. Sinyukov, "Femtoscopic scales in $p + p$ and $p + $Pb collisions in view of the uncertainty principle", *Phys. Lett. B* **725** (2013) 139, `doi:10.1016/j.physletb.2013.07.002`, `arXiv:1304.3815`.

[53] J. C. Collins and M. J. Perry, "Superdense matter: neutrons or asymptotically free quarks?", *Phys. Rev. Lett.* **34** (1975) 1353, `doi:10.1103/PhysRevLett.34.1353`.

[54] N. Cabibbo and G. Parisi, "Exponential hadronic spectrum and quark liberation", *Phys. Lett. B* **59** (1975) 67, `doi:10.1016/0370-2693(75)90158-6`.

[55] B. A. Freedman and L. D. McLerran, "Fermions and gauge vector mesons at finite temperature and density. 1. Formal techniques", *Phys. Rev. D* **16** (1977) 1130, `doi:10.1103/PhysRevD.16.1130`.

[56] E. V. Shuryak, "Theory of hadronic plasma", *Sov. Phys. JETP* **47** (1978) 212. [Zh. Eksp. Teor. Fiz. 74 (1978) 408].

[57] M. I. Khalatnikov, "Some questions onf the relativistic hydrodynamic", *Zh. Eksp. Teor. Fiz.* **26** (1954) 529.

[58] L. D. Landau, "On the multiple production of particles in high energy collisions", *Izv. Adak. Nauk SSSR Ser. Fiz.* **17** (1953) 51.

[59] R. Campanini and G. Ferri, "Experimental equation of state in pp and p$\overline{\text{p}}$ collisions and phase transition to quark gluon plasma", *Phys. Lett. B* **703** (2011) 237, `doi:10.1016/j.physletb.2011.08.009`, `arXiv:1106.2008`.

[60] G. Gräf, M. Bleicher, and Q. Li, "Examination of scaling of Hanbury-Brown–Twiss radii with charged particle multiplicity", *Phys. Rev. C* **85** (2012) 044901, `doi:10.1103/PhysRevC.85.044901,arXiv:1203.4071v2`.

[61] L. McLerran, M. Praszalowicz, and B. Schenke, "Transverse momentum of protons, pions and kaons in high multiplicity pp and pa collisions: evidence for the color glass condensate?", *Nucl. Phys. A* **916** (2013) 210, `doi:10.1016/j.nuclphysa.2013.08.008,arXiv:1306.2350`.

[62] A. Bzdak, B. Schenke, P. Tribedy, and R. Venugopalan, "Initial-state geometry and the role of hydrodynamics in proton-proton, proton-nucleus, and deuteron-nucleus collisions", *Phys. Rev. C* **87** (2013) 064906, `doi:10.1103/PhysRevC.87.064906`, `arXiv:1304.3403`.

[63] M. Chojnacki, W. Florkowski, and T. Csörgő, "Formation of Hubble-like flow in little bangs", *Phys. Rev. C* **71** (2005) 044902, `doi:10.1103/PhysRevC.71.044902`, `arXiv:nucl-th/0410036`.

[64] T. Csörgő and B. Lörstad, "Bose-Einstein correlations for three-dimensionally expanding, cylindrically symmetric, finite systems", *Phys. Rev. C* **54** (1996) 1390, `doi:10.1103/PhysRevC.54.1390,arXiv:hep-ph/9509213`.

[65] PHENIX Collaboration, "Bose-Einstein correlations of charged pion pairs in Au+Au collisions at $\sqrt{s_{NN}}$ = 200 GeV", *Phys. Rev. Lett.* **93** (2004) 152302, `doi:10.1103/PhysRevLett.93.152302,arXiv:nucl-ex/0401003`.

[66] STAR Collaboration, "Pion interferometry in Au+Au and Cu+Cu collisions at $\sqrt{s_{NN}}$ = 62.4 and 200 GeV", *Phys. Rev. C* **80** (2009) 024905, `doi:10.1103/PhysRevC.80.024905,arXiv:0903.1296`.

[67] PHENIX Collaboration, "Systematic study of charged-pion and kaon femtoscopy in Au+Au collisions at $\sqrt{s_{NN}}$ = 200 GeV", *Phys. Rev. C* **92** (2015) 034914, `doi:10.1103/PhysRevC.92.034914,arXiv:1504.05168`.

[68] ZEUS Collaboration, "Bose-Einstein correlations in one and two-dimensions in deep inelastic scattering", *Phys. Lett. B* **583** (2004) 231, `doi:10.1016/j.physletb.2003.12.068,arXiv:hep-ex/0311030`.

[69] L3 Collaboration, "Test of the τ-model of Bose-Einstein correlations and reconstruction of the source function in hadronic Z-boson decay at LEP", *Eur. Phys. J. C* **71** (2011) 1648, `doi:10.1140/epjc/s10052-011-1648-8,arXiv:1105.4788`.

[70] T. Csörgő and J. Zimányi, "Pion interferometry for strongly correlated space-time and momentum space", *Nucl. Phys. A* **517** (1990) 588, `doi:10.1016/0375-9474(90)90220-G`.

A Double ratios and cluster subtraction techniques

The analysis procedure using the double ratio (DR) technique follows Refs. [3–5]. For illustrating the procedure, Fig. 8 shows the single ratio (SR) defined in data, the one defined in simulation, as well as the DR. The reference sample used is the η-mixing sample defined previously, and the MC tune adopted is PYTHIA 6 Z2*. Both these choices are the default ones employed for obtaining the results in the DR method.
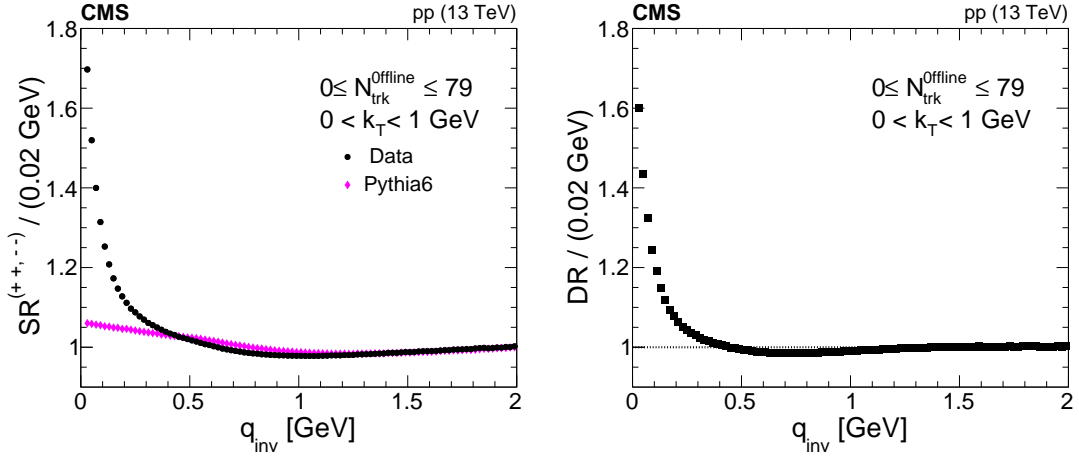

Figure 8: Illustration of the steps in the double ratio method. The single ratio in data is constructed (left), followed by a similar procedure with simulated events (PYTHIA 6, Z2* tune). The ratio of the two curves on the left defines the double ratio (right). The reference sample is obtained with the η-mixing procedure. All results correspond to integrated values in $N_{\mathrm{trk}}^{\mathrm{offline}}$ and k_{T}.

For obtaining the parameters of the BEC effect in this method, a DR is defined as

$$\mathrm{DR}(q_{\mathrm{inv}}) \equiv C_{2,\mathrm{BE}}(q_{\mathrm{inv}}) = \frac{\mathrm{SR}(q_{\mathrm{inv}})}{\mathrm{SR}(q_{\mathrm{inv}})_{\mathrm{MC}}} = \frac{\left[\left(\frac{\mathcal{N}_{\mathrm{ref}}}{\mathcal{N}_{\mathrm{sig}}}\right)\left(\frac{\mathrm{d}N_{\mathrm{sig}}/\mathrm{d}q_{\mathrm{inv}}}{\mathrm{d}N_{\mathrm{ref}}/\mathrm{d}q_{\mathrm{inv}}}\right)\right]}{\left[\left(\frac{\mathcal{N}_{\mathrm{ref}}}{\mathcal{N}_{\mathrm{sig}}}\right)_{\mathrm{MC}}\left(\frac{\mathrm{d}N_{\mathrm{MC}}/\mathrm{d}q_{\mathrm{inv}}}{\mathrm{d}N_{\mathrm{MC,\,ref}}/\mathrm{d}q_{\mathrm{inv}}}\right)\right]}, \tag{9}$$

where $C_{2,\mathrm{BE}}$ refers to the two-particle BEC, $\mathrm{SR}(q_{\mathrm{inv}})_{\mathrm{MC}}$ is the SR in Eq. (1), but computed with simulated events without BEC effects. In each case, the reference samples for data and simulation are constructed in the same way by considering all charged particles instead of only charged pions in the MC.

The DR method was used in Refs. [3–5] to reduce the bias due to the construction of the reference sample. The DR technique also has the advantage of reducing the non-BEC background that could remain in the SR (i.e., correlations coming from resonance decays and from energy-momentum conservation are not included in the reference sample, which is constructed with the event mixing technique adopted throughout this analysis). Therefore, by selecting a MC simulation that describes well the general properties of the data, those residual correlations can, in principle, be removed by taking the DRs with an SR defined similarly in MC events from non-BEC contributions [68, 69]).

The CS method, as described in Ref. [5], employs a different approach by dealing with only SRs, where contaminations (called "cluster contribution") from resonances and jet fragmentation are still present [17, 19, 49]. For the purpose of evaluating and removing such cluster effects, the one-dimensional opposite-sign (OS) SR correlation functions are fitted with the expression in
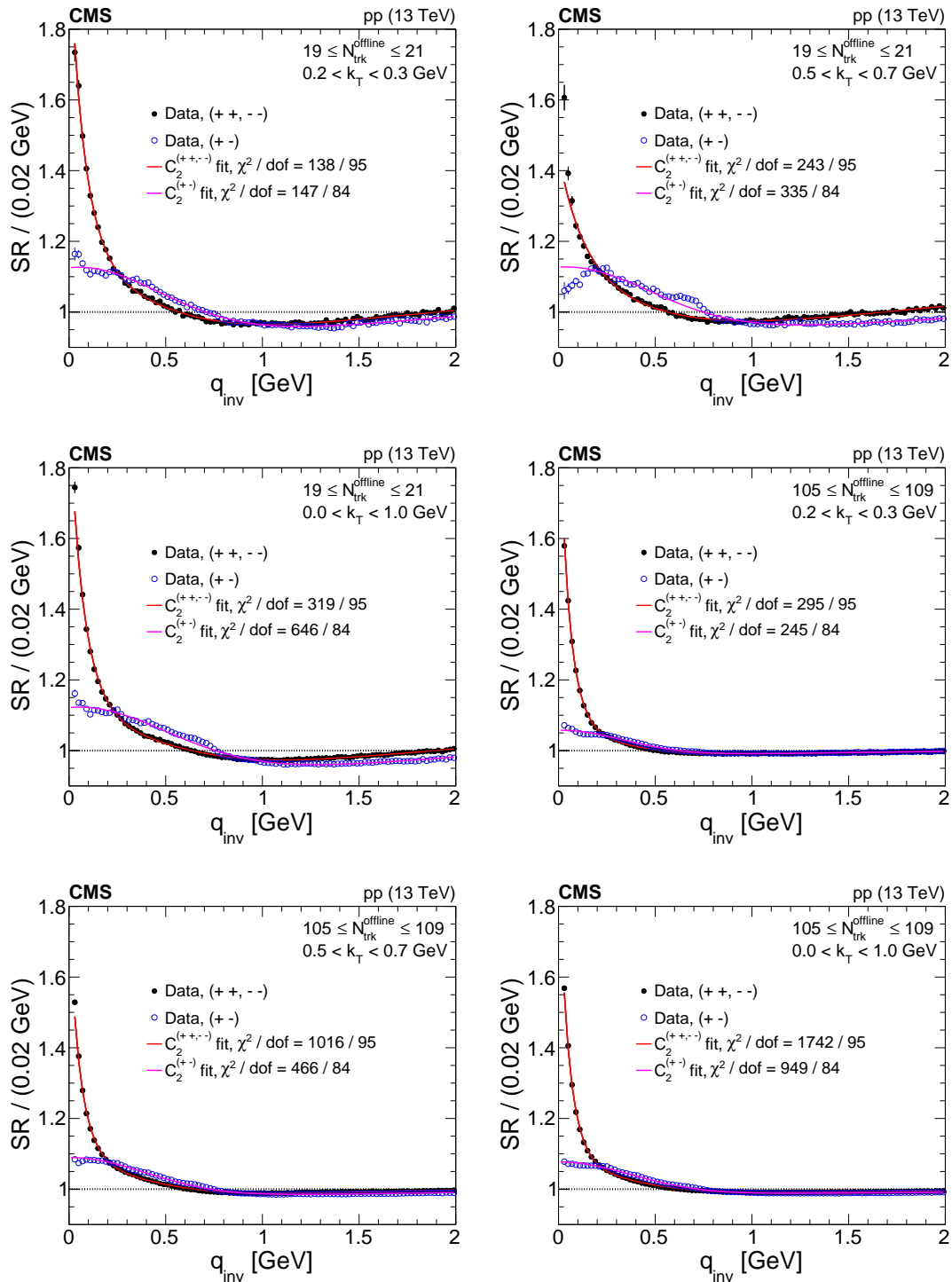
Figure 9: The same-sign $(++, --)$ and opposite-sign $(+-)$ single ratios are shown in different $N_{\mathrm{trk}}^{\mathrm{offline}}$ and k_{T} bins, together with the full fits (continuous curves) given in Eqs. (10) and (13), for minimum-bias $(19 \leq N_{\mathrm{trk}}^{\mathrm{offline}} \leq 21)$ and HM $(105 \leq N_{\mathrm{trk}}^{\mathrm{offline}} \leq 109)$ events. The error bars represent statistical uncertainties and in most cases are smaller than the marker size.

Eq. (10), which describes the data in all k_T and $N_{trk}^{offline}$ ranges (examples illustrating such fits are shown in Fig. 9),

$$C_2^{(+-)}(q_{inv}) = c \left[1 + \frac{b}{\sigma_b \sqrt{2\pi}} \exp \left(-\frac{q_{inv}^2}{2\sigma_b^2} \right) \right] (1 + \epsilon q_{inv}), \tag{10}$$

where b and σ_b are $N_{trk}^{offline}$- and k_T- dependent parameters, and c is an overall normalization constant, and $C_2^{(+-)}(q_{inv})$ refers to the opposite-sign correlation function. To avoid regions with substantial resonance contamination in the OS correlation function, the ranges $0.60 < q_{inv} < 0.80\,\text{GeV}$ and $q_{inv} < 0.04\,\text{GeV}$ are not used in the fits due to the $\rho(770)$ and photon conversion contributions, respectively; b and σ_b are parametrized as in Eqs. (11) and (12), respectively. Results of the fits using these parameterizations are shown in Table 2.

$$b(N_{trk}^{offline}, k_T) = \frac{b_0}{\left(N_{trk}^{offline}\right)^{n_b}} \exp \left(\frac{k_T}{k_0} \right); \tag{11}$$

$$\sigma_b(N_{trk}^{offline}, k_T) = \left[\sigma_0 + \sigma_1 \exp \left(-\frac{N_{trk}^{offline}}{N_0} \right) \right] k_T^{n_T}. \tag{12}$$

Table 2: Values of the fit parameters from Eqs. (11) and (12), describing the cluster contribution in the data OS correlation function. The estimated uncertainty in the parameters is about 10%.

b_0	n_b	k_0	σ_0	σ_1	N_0	n_T
0.90	0.55	0.8	0.35	0.30	64	0.081

Once the values of b and σ_b are determined from OS SR, the cluster contamination in the SS SR correlation function can be estimated. However, an important element, the conservation of electric charge in both minijet and multibody resonance decays, results in a stronger correlation (reflected in the parameter b), for the OS pairs than for the corresponding SS ones. Therefore, the form of the cluster-related contribution obtained from OS pairs is used to fit the SS correlations, but multiplied by an amplitude $z(N_{trk}^{offline}, k_T)$.

The expression in Eq. (13) is first used to fit the same-sign (SS) SRs for finding $z(N_{trk}^{offline}, k_T)$. The values obtained for the cluster amplitude are fitted for each k_T bin by a theoretically-motivated parametrization $[(a_1 N_{trk}^{offline} + b_1)/(1 + a_1 N_{trk}^{offline} + b_1)]$ [5], based on the ratio of the combinatorics of SS and OS particle pairs. Finally, this parametrization is employed in Eq. (13) for expressing $z(N_{trk}^{offline}, k_T)$ and refitting the SRs. For this fit, all the other variables (i.e., b, σ_b, z), given by the parameters obtained in earlier steps of the procedure, are kept fixed and only the overall normalization, c, and the parameters of the BEC function, $C_{BEC}(q_{inv})$, are fitted. In Fig. 9 some examples of correlation functions with the respective full fits, as in Eq.(13), are shown:

$$C_2^{(++,--)}(q_{inv}) = c \left[1 + z(N_{trk}^{offline}, k_T) \frac{b}{\sigma_b \sqrt{2\pi}} \exp \left(-\frac{q_{inv}^2}{2\sigma_b^2} \right) \right] C_{2,BE}(q_{inv}), \tag{13}$$

where $C_2^{(++,--)}(q_{inv})$ and $C_{2,BE}(q_{inv})$ refer to the same-sign correlation function and to the BEC, respectively.

B   Investigation of an observed anticorrelation

In previous CMS analyses [4, 5], the presence of an anticorrelation (dip) in the BEC functions was reported in pp collisions with characteristics that did not show a clear dependence on the center-of-mass energy. The DR technique is used for studying this behavior for pp collisions at 13 TeV since the two methods based on control samples in data include both the BEC and non-BEC contributions together in the fits, making it harder to disentangle these two components.

In Fig. 10, the DRs (zoomed along the correlation function axis) are illustrated in six ranges of multiplicity, for increasing values of $N_{\mathrm{trk}}^{\mathrm{offline}}$, ranging from MB to HM events. An anticorrelation is also observed in this case, being more pronounced in the lower $N_{\mathrm{trk}}^{\mathrm{offline}}$ bins. Prior to its observation in pp collisions, this anticorrelation had been seen in e^+e^- collisions [69], with features compatible with a description provided by the τ-model [70], in which particle production has a broad distribution in proper time and the phase space distribution of the emitted particles is dominated by strong correlations of the space-time coordinate and momentum components. Thus, this observation in MB pp collisions suggests that such structure could be associated with small systems. More details and related discussions can be found in Ref. [5].

The plots in Fig. 10 show the data points together with the exponential fit (continuous red curve) and a fit based on the τ-model (continuous green curve), which better describes the shape of the dip. Nevertheless, it should be noted that the χ^2 from both the τ-model and the exponential fits are large for some multiplicity bins, favoring neither one of these descriptions. On the other hand, this could also reflect the fact that the uncertainties coming from the choice of MC models are not included in the fits.

The depth of the anticorrelation, Δ, can be quantified [4, 5] with respect to the baseline represented by the polynomial form $C(1 + \epsilon\, q)$, as in Eq. (3), and the value of the curve corresponding to the τ-model fit at its minimum (details can be found in Ref. [5]). The corresponding results are shown in Fig. 11. The plot on the left shows the variation of Δ as a function of N_{tracks}, for integrated values of k_{T}. The depth of the dip decreases with multiplicity and suggest an approach to a constant value above $\langle N_{\mathrm{tracks}} \rangle \sim 120$. The behavior of the depth is shown as a function of k_{T} in the right plot, for several $N_{\mathrm{trk}}^{\mathrm{offline}}$ bins. In the lowest multiplicity bin, a clear decrease with k_{T} is seen, but the slope decreases as $N_{\mathrm{trk}}^{\mathrm{offline}}$ increases. The results for $60 < N_{\mathrm{trk}}^{\mathrm{offline}} < 80$ show a weak k_{T} dependence and the values of Δ are almost constant for $80 < N_{\mathrm{trk}}^{\mathrm{offline}} < 140$.

The fact that the depth of the dip, although small, seems to tend to a constant value different from zero at the highest measured multiplicities raises the question of this effect being a consequence of the DR method or an intrinsic characteristic of the collision system that could keep memory of its initially small size, even at the highest track multiplicities produced so far in pp collisions.
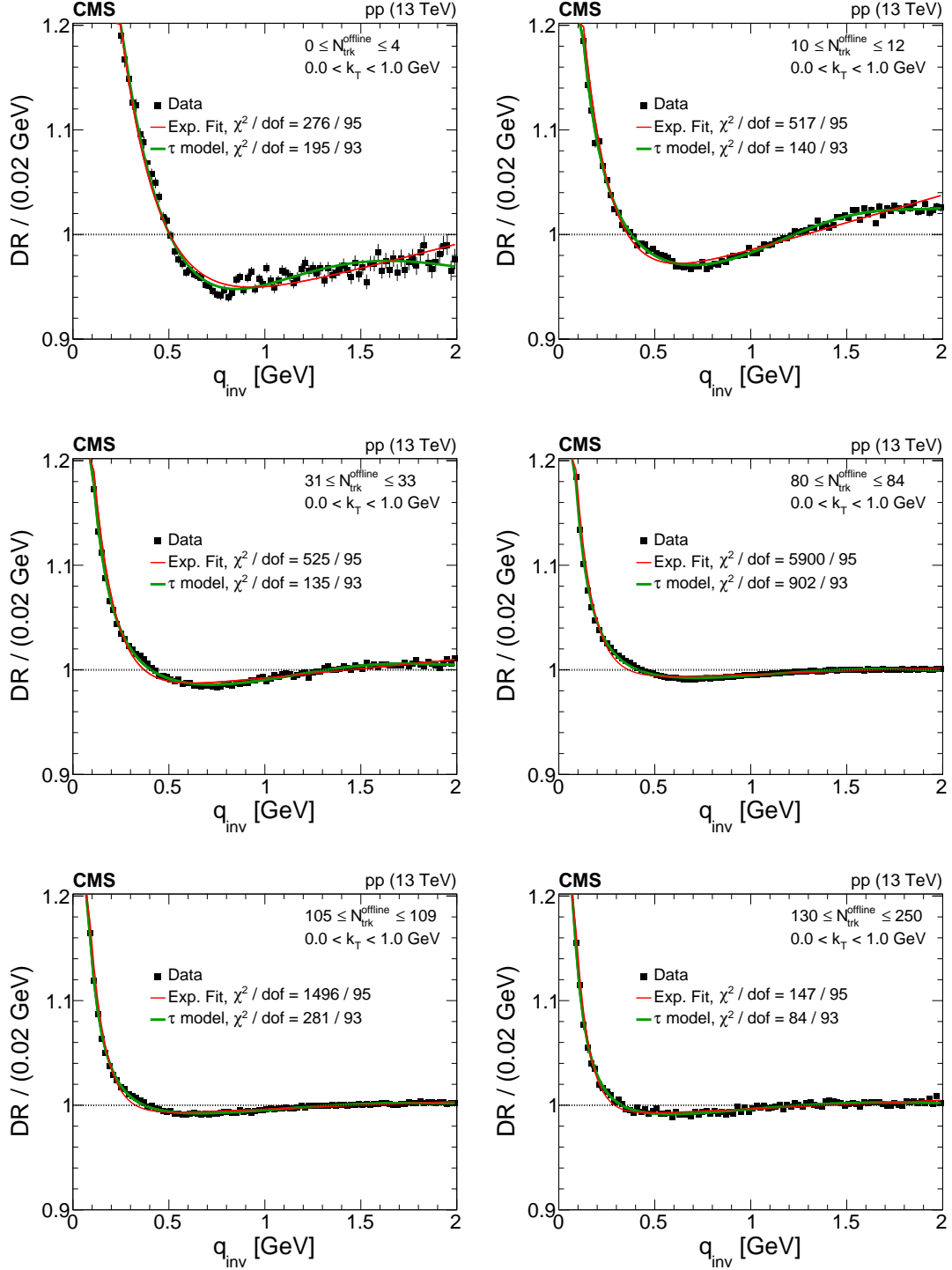
Figure 10: Correlation functions from the double ratio technique, integrated in the range $0 < k_T < 1\,\text{GeV}$, in six multiplicity bins. The results are zoomed along the vertical axis. The error bars represent statistical uncertainties and in most cases are smaller than the marker size.
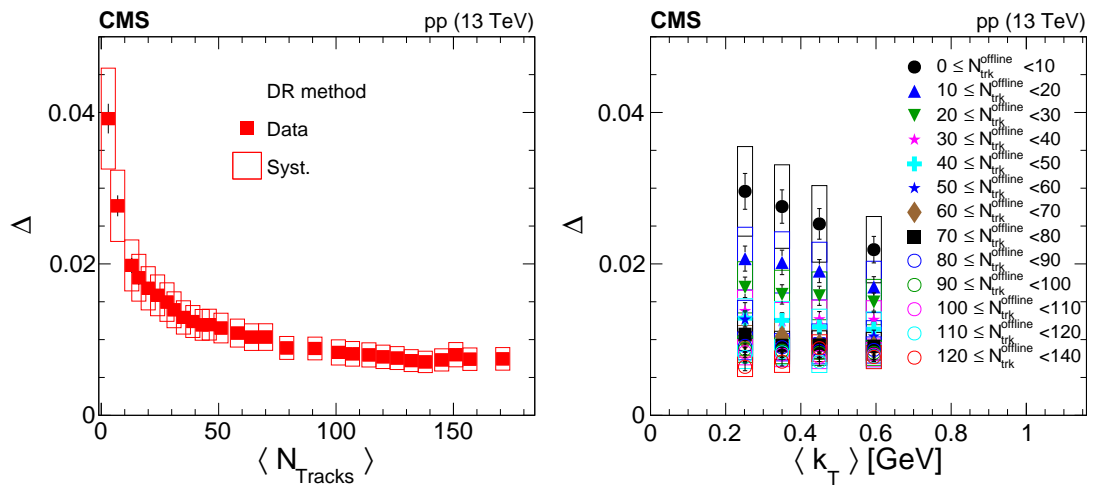
Figure 11: The depth of the anticorrelation Δ is shown as a function of multiplicity (left) for k_T-integrated values. The fit parameter Δ is also shown in finer bins of N_{tracks} and k_T (right). The statistical uncertainties are represented by the error bars, while the systematic ones are represented by the open boxes.

C The CMS Collaboration

Yerevan Physics Institute, Yerevan, Armenia
A.M. Sirunyan, A. Tumasyan

Institut für Hochenergiephysik, Wien, Austria
W. Adam, F. Ambrogi, E. Asilar, T. Bergauer, J. Brandstetter, M. Dragicevic, J. Erö, A. Escalante Del Valle, M. Flechl, R. Frühwirth[1], V.M. Ghete, J. Hrubec, M. Jeitler[1], N. Krammer, I. Krätschmer, D. Liko, T. Madlener, I. Mikulec, N. Rad, H. Rohringer, J. Schieck[1], R. Schöfbeck, M. Spanring, D. Spitzbart, A. Taurok, W. Waltenberger, J. Wittmann, C.-E. Wulz[1], M. Zarucki

Institute for Nuclear Problems, Minsk, Belarus
V. Chekhovsky, V. Mossolov, J. Suarez Gonzalez

Universiteit Antwerpen, Antwerpen, Belgium
E.A. De Wolf, D. Di Croce, X. Janssen, J. Lauwers, M. Pieters, H. Van Haevermaet, P. Van Mechelen, N. Van Remortel

Vrije Universiteit Brussel, Brussel, Belgium
S. Abu Zeid, F. Blekman, J. D'Hondt, I. De Bruyn, J. De Clercq, K. Deroover, G. Flouris, D. Lontkovskyi, S. Lowette, I. Marchesini, S. Moortgat, L. Moreels, Q. Python, K. Skovpen, S. Tavernier, W. Van Doninck, P. Van Mulders, I. Van Parijs

Université Libre de Bruxelles, Bruxelles, Belgium
D. Beghin, B. Bilin, H. Brun, B. Clerbaux, G. De Lentdecker, H. Delannoy, B. Dorney, G. Fasanella, L. Favart, R. Goldouzian, A. Grebenyuk, A.K. Kalsi, T. Lenzi, J. Luetic, N. Postiau, E. Starling, L. Thomas, C. Vander Velde, P. Vanlaer, D. Vannerom, Q. Wang

Ghent University, Ghent, Belgium
T. Cornelis, D. Dobur, A. Fagot, M. Gul, I. Khvastunov[2], D. Poyraz, C. Roskas, D. Trocino, M. Tytgat, W. Verbeke, B. Vermassen, M. Vit, N. Zaganidis

Université Catholique de Louvain, Louvain-la-Neuve, Belgium
H. Bakhshiansohi, O. Bondu, S. Brochet, G. Bruno, C. Caputo, P. David, C. Delaere, M. Delcourt, B. Francois, A. Giammanco, G. Krintiras, V. Lemaitre, A. Magitteri, A. Mertens, M. Musich, K. Piotrzkowski, A. Saggio, M. Vidal Marono, S. Wertz, J. Zobec

Centro Brasileiro de Pesquisas Fisicas, Rio de Janeiro, Brazil
F.L. Alves, G.A. Alves, M. Correa Martins Junior, G. Correia Silva, C. Hensel, A. Moraes, M.E. Pol, P. Rebello Teles

Universidade do Estado do Rio de Janeiro, Rio de Janeiro, Brazil
E. Belchior Batista Das Chagas, W. Carvalho, J. Chinellato[3], E. Coelho, E.M. Da Costa, G.G. Da Silveira[4], D. De Jesus Damiao, C. De Oliveira Martins, S. Fonseca De Souza, H. Malbouisson, D. Matos Figueiredo, M. Melo De Almeida, C. Mora Herrera, L. Mundim, H. Nogima, W.L. Prado Da Silva, L.J. Sanchez Rosas, A. Santoro, A. Sznajder, M. Thiel, E.J. Tonelli Manganote[3], F. Torres Da Silva De Araujo, A. Vilela Pereira

Universidade Estadual Paulista [a], Universidade Federal do ABC [b], São Paulo, Brazil
S. Ahuja[a], C.A. Bernardes[a], L. Calligaris[a], T.R. Fernandez Perez Tomei[a], E.M. Gregores[b], P.G. Mercadante[b], S.F. Novaes[a], SandraS. Padula[a]

Institute for Nuclear Research and Nuclear Energy, Bulgarian Academy of Sciences, Sofia,

Bulgaria
A. Aleksandrov, R. Hadjiiska, P. Iaydjiev, A. Marinov, M. Misheva, M. Rodozov, M. Shopova, G. Sultanov

University of Sofia, Sofia, Bulgaria
A. Dimitrov, L. Litov, B. Pavlov, P. Petkov

Beihang University, Beijing, China
W. Fang[5], X. Gao[5], L. Yuan

Institute of High Energy Physics, Beijing, China
M. Ahmad, J.G. Bian, G.M. Chen, H.S. Chen, M. Chen, Y. Chen, C.H. Jiang, D. Leggat, H. Liao, Z. Liu, F. Romeo, S.M. Shaheen[6], A. Spiezia, J. Tao, Z. Wang, E. Yazgan, H. Zhang, S. Zhang[6], J. Zhao

State Key Laboratory of Nuclear Physics and Technology, Peking University, Beijing, China
Y. Ban, G. Chen, A. Levin, J. Li, L. Li, Q. Li, Y. Mao, S.J. Qian, D. Wang, Z. Xu

Tsinghua University, Beijing, China
Y. Wang

Universidad de Los Andes, Bogota, Colombia
C. Avila, A. Cabrera, C.A. Carrillo Montoya, L.F. Chaparro Sierra, C. Florez, C.F. González Hernández, M.A. Segura Delgado

University of Split, Faculty of Electrical Engineering, Mechanical Engineering and Naval Architecture, Split, Croatia
B. Courbon, N. Godinovic, D. Lelas, I. Puljak, T. Sculac

University of Split, Faculty of Science, Split, Croatia
Z. Antunovic, M. Kovac

Institute Rudjer Boskovic, Zagreb, Croatia
V. Brigljevic, D. Ferencek, K. Kadija, B. Mesic, A. Starodumov[7], T. Susa

University of Cyprus, Nicosia, Cyprus
M.W. Ather, A. Attikis, M. Kolosova, G. Mavromanolakis, J. Mousa, C. Nicolaou, F. Ptochos, P.A. Razis, H. Rykaczewski

Charles University, Prague, Czech Republic
M. Finger[8], M. Finger Jr.[8]

Escuela Politecnica Nacional, Quito, Ecuador
E. Ayala

Universidad San Francisco de Quito, Quito, Ecuador
E. Carrera Jarrin

Academy of Scientific Research and Technology of the Arab Republic of Egypt, Egyptian Network of High Energy Physics, Cairo, Egypt
H. Abdalla[9], A. Mahrous[10], A. Mohamed[11]

National Institute of Chemical Physics and Biophysics, Tallinn, Estonia
S. Bhowmik, A. Carvalho Antunes De Oliveira, R.K. Dewanjee, K. Ehataht, M. Kadastik, M. Raidal, C. Veelken

Department of Physics, University of Helsinki, Helsinki, Finland
P. Eerola, H. Kirschenmann, J. Pekkanen, M. Voutilainen

Helsinki Institute of Physics, Helsinki, Finland
J. Havukainen, J.K. Heikkilä, T. Järvinen, V. Karimäki, R. Kinnunen, T. Lampén, K. Lassila-Perini, S. Laurila, S. Lehti, T. Lindén, P. Luukka, T. Mäenpää, H. Siikonen, E. Tuominen, J. Tuominiemi

Lappeenranta University of Technology, Lappeenranta, Finland
T. Tuuva

IRFU, CEA, Université Paris-Saclay, Gif-sur-Yvette, France
M. Besancon, F. Couderc, M. Dejardin, D. Denegri, J.L. Faure, F. Ferri, S. Ganjour, A. Givernaud, P. Gras, G. Hamel de Monchenault, P. Jarry, C. Leloup, E. Locci, J. Malcles, G. Negro, J. Rander, A. Rosowsky, M.Ö. Sahin, M. Titov

Laboratoire Leprince-Ringuet, Ecole polytechnique, CNRS/IN2P3, Université Paris-Saclay, Palaiseau, France
A. Abdulsalam[12], C. Amendola, I. Antropov, F. Beaudette, P. Busson, C. Charlot, R. Granier de Cassagnac, I. Kucher, A. Lobanov, J. Martin Blanco, C. Martin Perez, M. Nguyen, C. Ochando, G. Ortona, P. Paganini, P. Pigard, J. Rembser, R. Salerno, J.B. Sauvan, Y. Sirois, A.G. Stahl Leiton, A. Zabi, A. Zghiche

Université de Strasbourg, CNRS, IPHC UMR 7178, Strasbourg, France
J.-L. Agram[13], J. Andrea, D. Bloch, J.-M. Brom, E.C. Chabert, V. Cherepanov, C. Collard, E. Conte[13], J.-C. Fontaine[13], D. Gelé, U. Goerlach, M. Jansová, A.-C. Le Bihan, N. Tonon, P. Van Hove

Centre de Calcul de l'Institut National de Physique Nucleaire et de Physique des Particules, CNRS/IN2P3, Villeurbanne, France
S. Gadrat

Université de Lyon, Université Claude Bernard Lyon 1, CNRS-IN2P3, Institut de Physique Nucléaire de Lyon, Villeurbanne, France
S. Beauceron, C. Bernet, G. Boudoul, N. Chanon, R. Chierici, D. Contardo, P. Depasse, H. El Mamouni, J. Fay, L. Finco, S. Gascon, M. Gouzevitch, G. Grenier, B. Ille, F. Lagarde, I.B. Laktineh, H. Lattaud, M. Lethuillier, L. Mirabito, S. Perries, A. Popov[14], V. Sordini, G. Touquet, M. Vander Donckt, S. Viret

Georgian Technical University, Tbilisi, Georgia
T. Toriashvili[15]

Tbilisi State University, Tbilisi, Georgia
I. Bagaturia[16]

RWTH Aachen University, I. Physikalisches Institut, Aachen, Germany
C. Autermann, L. Feld, M.K. Kiesel, K. Klein, M. Lipinski, M. Preuten, M.P. Rauch, C. Schomakers, J. Schulz, M. Teroerde, B. Wittmer, V. Zhukov[14]

RWTH Aachen University, III. Physikalisches Institut A, Aachen, Germany
A. Albert, D. Duchardt, M. Endres, M. Erdmann, S. Ghosh, A. Güth, T. Hebbeker, C. Heidemann, K. Hoepfner, H. Keller, L. Mastrolorenzo, M. Merschmeyer, A. Meyer, P. Millet, S. Mukherjee, T. Pook, M. Radziej, H. Reithler, M. Rieger, A. Schmidt, D. Teyssier

RWTH Aachen University, III. Physikalisches Institut B, Aachen, Germany
G. Flügge, O. Hlushchenko, T. Kress, A. Künsken, T. Müller, A. Nehrkorn, A. Nowack, C. Pistone, O. Pooth, D. Roy, H. Sert, A. Stahl[17]

Deutsches Elektronen-Synchrotron, Hamburg, Germany
M. Aldaya Martin, T. Arndt, C. Asawatangtrakuldee, I. Babounikau, K. Beernaert, O. Behnke, U. Behrens, A. Bermúdez Martínez, D. Bertsche, A.A. Bin Anuar, K. Borras[18], V. Botta, A. Campbell, P. Connor, C. Contreras-Campana, V. Danilov, A. De Wit, M.M. Defranchis, C. Diez Pardos, D. Domínguez Damiani, G. Eckerlin, T. Eichhorn, A. Elwood, E. Eren, E. Gallo[19], A. Geiser, A. Grohsjean, M. Guthoff, M. Haranko, A. Harb, J. Hauk, H. Jung, M. Kasemann, J. Keaveney, C. Kleinwort, J. Knolle, D. Krücker, W. Lange, A. Lelek, T. Lenz, J. Leonard, K. Lipka, W. Lohmann[20], R. Mankel, I.-A. Melzer-Pellmann, A.B. Meyer, M. Meyer, M. Missiroli, G. Mittag, J. Mnich, V. Myronenko, S.K. Pflitsch, D. Pitzl, A. Raspereza, M. Savitskyi, P. Saxena, P. Schütze, C. Schwanenberger, R. Shevchenko, A. Singh, H. Tholen, O. Turkot, A. Vagnerini, G.P. Van Onsem, R. Walsh, Y. Wen, K. Wichmann, C. Wissing, O. Zenaiev

University of Hamburg, Hamburg, Germany
R. Aggleton, S. Bein, L. Benato, A. Benecke, V. Blobel, T. Dreyer, E. Garutti, D. Gonzalez, P. Gunnellini, J. Haller, A. Hinzmann, A. Karavdina, G. Kasieczka, R. Klanner, R. Kogler, N. Kovalchuk, S. Kurz, V. Kutzner, J. Lange, D. Marconi, J. Multhaup, M. Niedziela, C.E.N. Niemeyer, D. Nowatschin, A. Perieanu, A. Reimers, O. Rieger, C. Scharf, P. Schleper, S. Schumann, J. Schwandt, J. Sonneveld, H. Stadie, G. Steinbrück, F.M. Stober, M. Stöver, A. Vanhoefer, B. Vormwald, I. Zoi

Karlsruher Institut fuer Technologie, Karlsruhe, Germany
M. Akbiyik, C. Barth, M. Baselga, S. Baur, E. Butz, R. Caspart, T. Chwalek, F. Colombo, W. De Boer, A. Dierlamm, K. El Morabit, N. Faltermann, B. Freund, M. Giffels, M.A. Harrendorf, F. Hartmann[17], S.M. Heindl, U. Husemann, F. Kassel[17], I. Katkov[14], S. Kudella, H. Mildner, S. Mitra, M.U. Mozer, Th. Müller, M. Plagge, G. Quast, K. Rabbertz, M. Schröder, I. Shvetsov, G. Sieber, H.J. Simonis, R. Ulrich, S. Wayand, M. Weber, T. Weiler, S. Williamson, C. Wöhrmann, R. Wolf

Institute of Nuclear and Particle Physics (INPP), NCSR Demokritos, Aghia Paraskevi, Greece
G. Anagnostou, G. Daskalakis, T. Geralis, A. Kyriakis, D. Loukas, G. Paspalaki, I. Topsis-Giotis

National and Kapodistrian University of Athens, Athens, Greece
G. Karathanasis, S. Kesisoglou, P. Kontaxakis, A. Panagiotou, I. Papavergou, N. Saoulidou, E. Tziaferi, K. Vellidis

National Technical University of Athens, Athens, Greece
K. Kousouris, I. Papakrivopoulos, G. Tsipolitis

University of Ioánnina, Ioánnina, Greece
I. Evangelou, C. Foudas, P. Gianneios, P. Katsoulis, P. Kokkas, S. Mallios, N. Manthos, I. Papadopoulos, E. Paradas, J. Strologas, F.A. Triantis, D. Tsitsonis

MTA-ELTE Lendület CMS Particle and Nuclear Physics Group, Eötvös Loránd University, Budapest, Hungary
M. Bartók[21], M. Csanad, N. Filipovic, P. Major, M.I. Nagy, G. Pasztor, O. Surányi, G.I. Veres

Wigner Research Centre for Physics, Budapest, Hungary

G. Bencze, C. Hajdu, D. Horvath[22], . Hunyadi, F. Sikler, T.. Vámi, V. Veszpremi, G. Vesztergombi[†]

Institute of Nuclear Research ATOMKI, Debrecen, Hungary
N. Beni, S. Czellar, J. Karancsi[23], A. Makovec, J. Molnar, Z. Szillasi

Institute of Physics, University of Debrecen, Debrecen, Hungary
P. Raics, Z.L. Trocsanyi, B. Ujvari

Indian Institute of Science (IISc), Bangalore, India
S. Choudhury, J.R. Komaragiri, P.C. Tiwari

National Institute of Science Education and Research, HBNI, Bhubaneswar, India
S. Bahinipati[24], C. Kar, P. Mal, K. Mandal, A. Nayak[25], D.K. Sahoo[24], S.K. Swain

Panjab University, Chandigarh, India
S. Bansal, S.B. Beri, V. Bhatnagar, S. Chauhan, R. Chawla, N. Dhingra, R. Gupta, A. Kaur, M. Kaur, S. Kaur, R. Kumar, P. Kumari, M. Lohan, A. Mehta, K. Sandeep, S. Sharma, J.B. Singh, A.K. Virdi, G. Walia

University of Delhi, Delhi, India
A. Bhardwaj, B.C. Choudhary, R.B. Garg, M. Gola, S. Keshri, Ashok Kumar, S. Malhotra, M. Naimuddin, P. Priyanka, K. Ranjan, Aashaq Shah, R. Sharma

Saha Institute of Nuclear Physics, HBNI, Kolkata, India
R. Bhardwaj[26], M. Bharti[26], R. Bhattacharya, S. Bhattacharya, U. Bhawandeep[26], D. Bhowmik, S. Dey, S. Dutt[26], S. Dutta, S. Ghosh, K. Mondal, S. Nandan, A. Purohit, P.K. Rout, A. Roy, S. Roy Chowdhury, G. Saha, S. Sarkar, M. Sharan, B. Singh[26], S. Thakur[26]

Indian Institute of Technology Madras, Madras, India
P.K. Behera

Bhabha Atomic Research Centre, Mumbai, India
R. Chudasama, D. Dutta, V. Jha, V. Kumar, P.K. Netrakanti, L.M. Pant, P. Shukla

Tata Institute of Fundamental Research-A, Mumbai, India
T. Aziz, M.A. Bhat, S. Dugad, G.B. Mohanty, N. Sur, B. Sutar, RavindraKumar Verma

Tata Institute of Fundamental Research-B, Mumbai, India
S. Banerjee, S. Bhattacharya, S. Chatterjee, P. Das, M. Guchait, Sa. Jain, S. Karmakar, S. Kumar, M. Maity[27], G. Majumder, K. Mazumdar, N. Sahoo, T. Sarkar[27]

Indian Institute of Science Education and Research (IISER), Pune, India
S. Chauhan, S. Dube, V. Hegde, A. Kapoor, K. Kothekar, S. Pandey, A. Rane, S. Sharma

Institute for Research in Fundamental Sciences (IPM), Tehran, Iran
S. Chenarani[28], E. Eskandari Tadavani, S.M. Etesami[28], M. Khakzad, M. Mohammadi Najafabadi, M. Naseri, F. Rezaei Hosseinabadi, B. Safarzadeh[29], M. Zeinali

University College Dublin, Dublin, Ireland
M. Felcini, M. Grunewald

INFN Sezione di Bari ^{a}, Università di Bari ^{b}, Politecnico di Bari ^{c}, Bari, Italy
M. Abbrescia^{a,b}, C. Calabria^{a,b}, A. Colaleo^a, D. Creanza^{a,c}, L. Cristella^{a,b}, N. De Filippis^{a,c}, M. De Palma^{a,b}, A. Di Florio^{a,b}, F. Errico^{a,b}, L. Fiore^a, A. Gelmi^{a,b}, G. Iaselli^{a,c}, M. Ince^{a,b}, S. Lezki^{a,b}, G. Maggi^{a,c}, M. Maggi^a, G. Miniello^{a,b}, S. My^{a,b}, S. Nuzzo^{a,b}, A. Pompili^{a,b},

G. Pugliese[a,c], R. Radogna[a], A. Ranieri[a], G. Selvaggi[a,b], A. Sharma[a], L. Silvestris[a], R. Venditti[a], P. Verwilligen[a], G. Zito[a]

INFN Sezione di Bologna [a], Università di Bologna [b], Bologna, Italy
G. Abbiendi[a], C. Battilana[a,b], D. Bonacorsi[a,b], L. Borgonovi[a,b], S. Braibant-Giacomelli[a,b], R. Campanini[a,b], P. Capiluppi[a,b], A. Castro[a,b], F.R. Cavallo[a], S.S. Chhibra[a,b], C. Ciocca[a], G. Codispoti[a,b], M. Cuffiani[a,b], G.M. Dallavalle[a], F. Fabbri[a], A. Fanfani[a,b], E. Fontanesi, P. Giacomelli[a], C. Grandi[a], L. Guiducci[a,b], S. Lo Meo[a], S. Marcellini[a], G. Masetti[a], A. Montanari[a], F.L. Navarria[a,b], A. Perrotta[a], F. Primavera[a,b,17], A.M. Rossi[a,b], T. Rovelli[a,b], G.P. Siroli[a,b], N. Tosi[a]

INFN Sezione di Catania [a], Università di Catania [b], Catania, Italy
S. Albergo[a,b], A. Di Mattia[a], R. Potenza[a,b], A. Tricomi[a,b], C. Tuve[a,b]

INFN Sezione di Firenze [a], Università di Firenze [b], Firenze, Italy
G. Barbagli[a], K. Chatterjee[a,b], V. Ciulli[a,b], C. Civinini[a], R. D'Alessandro[a,b], E. Focardi[a,b], G. Latino, P. Lenzi[a,b], M. Meschini[a], S. Paoletti[a], L. Russo[a,30], G. Sguazzoni[a], D. Strom[a], L. Viliani[a]

INFN Laboratori Nazionali di Frascati, Frascati, Italy
L. Benussi, S. Bianco, F. Fabbri, D. Piccolo

INFN Sezione di Genova [a], Università di Genova [b], Genova, Italy
F. Ferro[a], F. Ravera[a,b], E. Robutti[a], S. Tosi[a,b]

INFN Sezione di Milano-Bicocca [a], Università di Milano-Bicocca [b], Milano, Italy
A. Benaglia[a], A. Beschi[b], L. Brianza[a,b], F. Brivio[a,b], V. Ciriolo[a,b,17], S. Di Guida[a,d,17], M.E. Dinardo[a,b], S. Fiorendi[a,b], S. Gennai[a], A. Ghezzi[a,b], P. Govoni[a,b], M. Malberti[a,b], S. Malvezzi[a], A. Massironi[a,b], D. Menasce[a], F. Monti, L. Moroni[a], M. Paganoni[a,b], D. Pedrini[a], S. Ragazzi[a,b], T. Tabarelli de Fatis[a,b], D. Zuolo[a,b]

INFN Sezione di Napoli [a], Università di Napoli 'Federico II' [b], Napoli, Italy, Università della Basilicata [c], Potenza, Italy, Università G. Marconi [d], Roma, Italy
S. Buontempo[a], N. Cavallo[a,c], A. Di Crescenzo[a,b], F. Fabozzi[a,c], F. Fienga[a], G. Galati[a], A.O.M. Iorio[a,b], W.A. Khan[a], L. Lista[a], S. Meola[a,d,17], P. Paolucci[a,17], C. Sciacca[a,b], E. Voevodina[a,b]

INFN Sezione di Padova [a], Università di Padova [b], Padova, Italy, Università di Trento [c], Trento, Italy
P. Azzi[a], N. Bacchetta[a], D. Bisello[a,b], A. Boletti[a,b], A. Bragagnolo, R. Carlin[a,b], P. Checchia[a], M. Dall'Osso[a,b], P. De Castro Manzano[a], T. Dorigo[a], U. Dosselli[a], F. Gasparini[a,b], U. Gasparini[a,b], A. Gozzelino[a], S.Y. Hoh, S. Lacaprara[a], P. Lujan, M. Margoni[a,b], A.T. Meneguzzo[a,b], J. Pazzini[a,b], P. Ronchese[a,b], R. Rossin[a,b], F. Simonetto[a,b], A. Tiko, E. Torassa[a], M. Zanetti[a,b], P. Zotto[a,b], G. Zumerle[a,b]

INFN Sezione di Pavia [a], Università di Pavia [b], Pavia, Italy
A. Braghieri[a], A. Magnani[a], P. Montagna[a,b], S.P. Ratti[a,b], V. Re[a], M. Ressegotti[a,b], C. Riccardi[a,b], P. Salvini[a], I. Vai[a,b], P. Vitulo[a,b]

INFN Sezione di Perugia [a], Università di Perugia [b], Perugia, Italy
M. Biasini[a,b], G.M. Bilei[a], C. Cecchi[a,b], D. Ciangottini[a,b], L. Fanò[a,b], P. Lariccia[a,b], R. Leonardi[a,b], E. Manoni[a], G. Mantovani[a,b], V. Mariani[a,b], M. Menichelli[a], A. Rossi[a,b], A. Santocchia[a,b], D. Spiga[a]

INFN Sezione di Pisa [a], Università di Pisa [b], Scuola Normale Superiore di Pisa [c], Pisa, Italy
K. Androsov[a], P. Azzurri[a], G. Bagliesi[a], L. Bianchini[a], T. Boccali[a], L. Borrello, R. Castaldi[a], M.A. Ciocci[a,b], R. Dell'Orso[a], G. Fedi[a], F. Fiori[a,c], L. Giannini[a,c], A. Giassi[a], M.T. Grippo[a], F. Ligabue[a,c], E. Manca[a,c], G. Mandorli[a,c], A. Messineo[a,b], F. Palla[a], A. Rizzi[a,b], P. Spagnolo[a], R. Tenchini[a], G. Tonelli[a,b], A. Venturi[a], P.G. Verdini[a]

INFN Sezione di Roma [a], Sapienza Università di Roma [b], Rome, Italy
L. Barone[a,b], F. Cavallari[a], M. Cipriani[a,b], D. Del Re[a,b], E. Di Marco[a,b], M. Diemoz[a], S. Gelli[a,b], E. Longo[a,b], B. Marzocchi[a,b], P. Meridiani[a], G. Organtini[a,b], F. Pandolfi[a], R. Paramatti[a,b], F. Preiato[a,b], S. Rahatlou[a,b], C. Rovelli[a], F. Santanastasio[a,b]

INFN Sezione di Torino [a], Università di Torino [b], Torino, Italy, Università del Piemonte Orientale [c], Novara, Italy
N. Amapane[a,b], R. Arcidiacono[a,c], S. Argiro[a,b], M. Arneodo[a,c], N. Bartosik[a], R. Bellan[a,b], C. Biino[a], N. Cartiglia[a], F. Cenna[a,b], S. Cometti[a], M. Costa[a,b], R. Covarelli[a,b], N. Demaria[a], B. Kiani[a,b], C. Mariotti[a], S. Maselli[a], E. Migliore[a,b], V. Monaco[a,b], E. Monteil[a,b], M. Monteno[a], M.M. Obertino[a,b], L. Pacher[a,b], N. Pastrone[a], M. Pelliccioni[a], G.L. Pinna Angioni[a,b], A. Romero[a,b], M. Ruspa[a,c], R. Sacchi[a,b], K. Shchelina[a,b], V. Sola[a], A. Solano[a,b], D. Soldi[a,b], A. Staiano[a]

INFN Sezione di Trieste [a], Università di Trieste [b], Trieste, Italy
S. Belforte[a], V. Candelise[a,b], M. Casarsa[a], F. Cossutti[a], A. Da Rold[a,b], G. Della Ricca[a,b], F. Vazzoler[a,b], A. Zanetti[a]

Kyungpook National University, Daegu, Korea
S. Dogra, D.H. Kim, G.N. Kim, M.S. Kim, J. Lee, S. Lee, S.W. Lee, C.S. Moon, Y.D. Oh, S.I. Pak, S. Sekmen, D.C. Son, Y.C. Yang

Chonnam National University, Institute for Universe and Elementary Particles, Kwangju, Korea
H. Kim, D.H. Moon, G. Oh

Hanyang University, Seoul, Korea
J. Goh[31], T.J. Kim

Korea University, Seoul, Korea
S. Cho, S. Choi, Y. Go, D. Gyun, S. Ha, B. Hong, Y. Jo, K. Lee, K.S. Lee, S. Lee, J. Lim, S.K. Park, Y. Roh

Sejong University, Seoul, Korea
H.S. Kim

Seoul National University, Seoul, Korea
J. Almond, J. Kim, J.S. Kim, H. Lee, K. Lee, K. Nam, S.B. Oh, B.C. Radburn-Smith, S.h. Seo, U.K. Yang, H.D. Yoo, G.B. Yu

University of Seoul, Seoul, Korea
D. Jeon, H. Kim, J.H. Kim, J.S.H. Lee, I.C. Park

Sungkyunkwan University, Suwon, Korea
Y. Choi, C. Hwang, J. Lee, I. Yu

Vilnius University, Vilnius, Lithuania
V. Dudenas, A. Juodagalvis, J. Vaitkus

National Centre for Particle Physics, Universiti Malaya, Kuala Lumpur, Malaysia
I. Ahmed, Z.A. Ibrahim, M.A.B. Md Ali[32], F. Mohamad Idris[33], W.A.T. Wan Abdullah, M.N. Yusli, Z. Zolkapli

Universidad de Sonora (UNISON), Hermosillo, Mexico
J.F. Benitez, A. Castaneda Hernandez, J.A. Murillo Quijada

Centro de Investigacion y de Estudios Avanzados del IPN, Mexico City, Mexico
H. Castilla-Valdez, E. De La Cruz-Burelo, M.C. Duran-Osuna, I. Heredia-De La Cruz[34], R. Lopez-Fernandez, J. Mejia Guisao, R.I. Rabadan-Trejo, M. Ramirez-Garcia, G. Ramirez-Sanchez, R Reyes-Almanza, A. Sanchez-Hernandez

Universidad Iberoamericana, Mexico City, Mexico
S. Carrillo Moreno, C. Oropeza Barrera, F. Vazquez Valencia

Benemerita Universidad Autonoma de Puebla, Puebla, Mexico
J. Eysermans, I. Pedraza, H.A. Salazar Ibarguen, C. Uribe Estrada

Universidad Autónoma de San Luis Potosí, San Luis Potosí, Mexico
A. Morelos Pineda

University of Auckland, Auckland, New Zealand
D. Krofcheck

University of Canterbury, Christchurch, New Zealand
S. Bheesette, P.H. Butler

National Centre for Physics, Quaid-I-Azam University, Islamabad, Pakistan
A. Ahmad, M. Ahmad, M.I. Asghar, Q. Hassan, H.R. Hoorani, A. Saddique, M.A. Shah, M. Shoaib, M. Waqas

National Centre for Nuclear Research, Swierk, Poland
H. Bialkowska, M. Bluj, B. Boimska, T. Frueboes, M. Górski, M. Kazana, K. Nawrocki, M. Szleper, P. Traczyk, P. Zalewski

Institute of Experimental Physics, Faculty of Physics, University of Warsaw, Warsaw, Poland
K. Bunkowski, A. Byszuk[35], K. Doroba, A. Kalinowski, M. Konecki, J. Krolikowski, M. Misiura, M. Olszewski, A. Pyskir, M. Walczak

Laboratório de Instrumentação e Física Experimental de Partículas, Lisboa, Portugal
M. Araujo, P. Bargassa, C. Beirão Da Cruz E Silva, A. Di Francesco, P. Faccioli, B. Galinhas, M. Gallinaro, J. Hollar, N. Leonardo, M.V. Nemallapudi, J. Seixas, G. Strong, O. Toldaiev, D. Vadruccio, J. Varela

Joint Institute for Nuclear Research, Dubna, Russia
S. Afanasiev, P. Bunin, M. Gavrilenko, I. Golutvin, I. Gorbunov, A. Kamenev, V. Karjavine, A. Lanev, A. Malakhov, V. Matveev[36,37], P. Moisenz, V. Palichik, V. Perelygin, S. Shmatov, S. Shulha, N. Skatchkov, V. Smirnov, N. Voytishin, A. Zarubin

Petersburg Nuclear Physics Institute, Gatchina (St. Petersburg), Russia
V. Golovtsov, Y. Ivanov, V. Kim[38], E. Kuznetsova[39], P. Levchenko, V. Murzin, V. Oreshkin, I. Smirnov, D. Sosnov, V. Sulimov, L. Uvarov, S. Vavilov, A. Vorobyev

Institute for Nuclear Research, Moscow, Russia
Yu. Andreev, A. Dermenev, S. Gninenko, N. Golubev, A. Karneyeu, M. Kirsanov, N. Krasnikov, A. Pashenkov, D. Tlisov, A. Toropin

Institute for Theoretical and Experimental Physics named by A.I. Alikhanov of NRC 'Kurchatov Institute', Moscow, Russia
V. Epshteyn, V. Gavrilov, N. Lychkovskaya, V. Popov, I. Pozdnyakov, G. Safronov, A. Spiridonov, A. Stepennov, V. Stolin, M. Toms, E. Vlasov, A. Zhokin

Moscow Institute of Physics and Technology, Moscow, Russia
T. Aushev

National Research Nuclear University 'Moscow Engineering Physics Institute' (MEPhI), Moscow, Russia
M. Chadeeva[40], P. Parygin, D. Philippov, S. Polikarpov[40], E. Popova, V. Rusinov

P.N. Lebedev Physical Institute, Moscow, Russia
V. Andreev, M. Azarkin[37], I. Dremin[37], M. Kirakosyan[37], S.V. Rusakov, A. Terkulov

Skobeltsyn Institute of Nuclear Physics, Lomonosov Moscow State University, Moscow, Russia
A. Baskakov, A. Belyaev, E. Boos, A. Ershov, A. Gribushin, L. Khein, V. Klyukhin, O. Kodolova, I. Lokhtin, O. Lukina, I. Miagkov, S. Obraztsov, S. Petrushanko, V. Savrin, A. Snigirev

Novosibirsk State University (NSU), Novosibirsk, Russia
A. Barnyakov[41], V. Blinov[41], T. Dimova[41], L. Kardapoltsev[41], Y. Skovpen[41]

Institute for High Energy Physics of National Research Centre 'Kurchatov Institute', Protvino, Russia
I. Azhgirey, I. Bayshev, S. Bitioukov, D. Elumakhov, A. Godizov, V. Kachanov, A. Kalinin, D. Konstantinov, P. Mandrik, V. Petrov, R. Ryutin, S. Slabospitskii, A. Sobol, S. Troshin, N. Tyurin, A. Uzunian, A. Volkov

National Research Tomsk Polytechnic University, Tomsk, Russia
A. Babaev, S. Baidali, V. Okhotnikov

University of Belgrade: Faculty of Physics and VINCA Institute of Nuclear Sciences
P. Adzic[42], P. Cirkovic, D. Devetak, M. Dordevic, J. Milosevic

Centro de Investigaciones Energéticas Medioambientales y Tecnológicas (CIEMAT), Madrid, Spain
J. Alcaraz Maestre, A. lvarez Fernández, I. Bachiller, M. Barrio Luna, J.A. Brochero Cifuentes, M. Cerrada, N. Colino, B. De La Cruz, A. Delgado Peris, C. Fernandez Bedoya, J.P. Fernández Ramos, J. Flix, M.C. Fouz, O. Gonzalez Lopez, S. Goy Lopez, J.M. Hernandez, M.I. Josa, D. Moran, A. Pérez-Calero Yzquierdo, J. Puerta Pelayo, I. Redondo, L. Romero, M.S. Soares, A. Triossi

Universidad Autónoma de Madrid, Madrid, Spain
C. Albajar, J.F. de Trocóniz

Universidad de Oviedo, Instituto Universitario de Ciencias y Tecnologías Espaciales de Asturias (ICTEA), Oviedo, Spain
J. Cuevas, C. Erice, J. Fernandez Menendez, S. Folgueras, I. Gonzalez Caballero, J.R. González Fernández, E. Palencia Cortezon, V. Rodríguez Bouza, S. Sanchez Cruz, P. Vischia, J.M. Vizan Garcia

Instituto de Física de Cantabria (IFCA), CSIC-Universidad de Cantabria, Santander, Spain
I.J. Cabrillo, A. Calderon, B. Chazin Quero, J. Duarte Campderros, M. Fernandez, P.J. Fernández Manteca, A. García Alonso, J. Garcia-Ferrero, G. Gomez, A. Lopez Virto,

J. Marco, C. Martinez Rivero, P. Martinez Ruiz del Arbol, F. Matorras, J. Piedra Gomez, C. Prieels, T. Rodrigo, A. Ruiz-Jimeno, L. Scodellaro, N. Trevisani, I. Vila, R. Vilar Cortabitarte

University of Ruhuna, Department of Physics, Matara, Sri Lanka
N. Wickramage

CERN, European Organization for Nuclear Research, Geneva, Switzerland
D. Abbaneo, B. Akgun, E. Auffray, G. Auzinger, P. Baillon, A.H. Ball, D. Barney, J. Bendavid, M. Bianco, A. Bocci, C. Botta, E. Brondolin, T. Camporesi, M. Cepeda, G. Cerminara, E. Chapon, Y. Chen, G. Cucciati, D. d'Enterria, A. Dabrowski, N. Daci, V. Daponte, A. David, A. De Roeck, N. Deelen, M. Dobson, M. Dünser, N. Dupont, A. Elliott-Peisert, P. Everaerts, F. Fallavollita[43], D. Fasanella, G. Franzoni, J. Fulcher, W. Funk, D. Gigi, A. Gilbert, K. Gill, F. Glege, M. Guilbaud, D. Gulhan, J. Hegeman, C. Heidegger, V. Innocente, A. Jafari, P. Janot, O. Karacheban[20], J. Kieseler, A. Kornmayer, M. Krammer[1], C. Lange, P. Lecoq, C. Lourenço, L. Malgeri, M. Mannelli, F. Meijers, J.A. Merlin, S. Mersi, E. Meschi, P. Milenovic[44], F. Moortgat, M. Mulders, J. Ngadiuba, S. Nourbakhsh, S. Orfanelli, L. Orsini, F. Pantaleo[17], L. Pape, E. Perez, M. Peruzzi, A. Petrilli, G. Petrucciani, A. Pfeiffer, M. Pierini, F.M. Pitters, D. Rabady, A. Racz, T. Reis, G. Rolandi[45], M. Rovere, H. Sakulin, C. Schäfer, C. Schwick, M. Seidel, M. Selvaggi, A. Sharma, P. Silva, P. Sphicas[46], A. Stakia, J. Steggemann, M. Tosi, D. Treille, A. Tsirou, V. Veckalns[47], M. Verzetti, W.D. Zeuner

Paul Scherrer Institut, Villigen, Switzerland
L. Caminada[48], K. Deiters, W. Erdmann, R. Horisberger, Q. Ingram, H.C. Kaestli, D. Kotlinski, U. Langenegger, T. Rohe, S.A. Wiederkehr

ETH Zurich - Institute for Particle Physics and Astrophysics (IPA), Zurich, Switzerland
M. Backhaus, L. Bäni, P. Berger, N. Chernyavskaya, G. Dissertori, M. Dittmar, M. Donegà, C. Dorfer, T.A. Gómez Espinosa, C. Grab, D. Hits, T. Klijnsma, W. Lustermann, R.A. Manzoni, M. Marionneau, M.T. Meinhard, F. Micheli, P. Musella, F. Nessi-Tedaldi, J. Pata, F. Pauss, G. Perrin, L. Perrozzi, S. Pigazzini, M. Quittnat, D. Ruini, D.A. Sanz Becerra, M. Schönenberger, L. Shchutska, V.R. Tavolaro, K. Theofilatos, M.L. Vesterbacka Olsson, R. Wallny, D.H. Zhu

Universität Zürich, Zurich, Switzerland
T.K. Aarrestad, C. Amsler[49], D. Brzhechko, M.F. Canelli, A. De Cosa, R. Del Burgo, S. Donato, C. Galloni, T. Hreus, B. Kilminster, S. Leontsinis, I. Neutelings, D. Pinna, G. Rauco, P. Robmann, D. Salerno, K. Schweiger, C. Seitz, Y. Takahashi, A. Zucchetta

National Central University, Chung-Li, Taiwan
Y.H. Chang, K.y. Cheng, T.H. Doan, Sh. Jain, R. Khurana, C.M. Kuo, W. Lin, A. Pozdnyakov, S.S. Yu

National Taiwan University (NTU), Taipei, Taiwan
P. Chang, Y. Chao, K.F. Chen, P.H. Chen, W.-S. Hou, Arun Kumar, Y.F. Liu, R.-S. Lu, E. Paganis, A. Psallidas, A. Steen

Chulalongkorn University, Faculty of Science, Department of Physics, Bangkok, Thailand
B. Asavapibhop, N. Srimanobhas, N. Suwonjandee

ukurova University, Physics Department, Science and Art Faculty, Adana, Turkey
A. Bat, F. Boran, S. Damarseckin, Z.S. Demiroglu, F. Dolek, C. Dozen, I. Dumanoglu, S. Girgis, G. Gokbulut, Y. Guler, E. Gurpinar, I. Hos[50], C. Isik, E.E. Kangal[51], O. Kara, A. Kayis Topaksu, U. Kiminsu, M. Oglakci, G. Onengut, K. Ozdemir[52], A. Polatoz, D. Sunar Cerci[53], B. Tali[53], U.G. Tok, H. Topakli[54], S. Turkcapar, I.S. Zorbakir, C. Zorbilmez

Middle East Technical University, Physics Department, Ankara, Turkey
B. Isildak[55], G. Karapinar[56], M. Yalvac, M. Zeyrek

Bogazici University, Istanbul, Turkey
I.O. Atakisi, E. Gülmez, M. Kaya[57], O. Kaya[58], S. Ozkorucuklu[59], S. Tekten, E.A. Yetkin[60]

Istanbul Technical University, Istanbul, Turkey
M.N. Agaras, A. Cakir, K. Cankocak, Y. Komurcu, S. Sen[61]

Institute for Scintillation Materials of National Academy of Science of Ukraine, Kharkov, Ukraine
B. Grynyov

National Scientific Center, Kharkov Institute of Physics and Technology, Kharkov, Ukraine
L. Levchuk

University of Bristol, Bristol, United Kingdom
F. Ball, L. Beck, J.J. Brooke, D. Burns, E. Clement, D. Cussans, O. Davignon, H. Flacher, J. Goldstein, G.P. Heath, H.F. Heath, L. Kreczko, D.M. Newbold[62], S. Paramesvaran, B. Penning, T. Sakuma, D. Smith, V.J. Smith, J. Taylor, A. Titterton

Rutherford Appleton Laboratory, Didcot, United Kingdom
K.W. Bell, A. Belyaev[63], C. Brew, R.M. Brown, D. Cieri, D.J.A. Cockerill, J.A. Coughlan, K. Harder, S. Harper, J. Linacre, E. Olaiya, D. Petyt, C.H. Shepherd-Themistocleous, A. Thea, I.R. Tomalin, T. Williams, W.J. Womersley

Imperial College, London, United Kingdom
R. Bainbridge, P. Bloch, J. Borg, S. Breeze, O. Buchmuller, A. Bundock, D. Colling, P. Dauncey, G. Davies, M. Della Negra, R. Di Maria, Y. Haddad, G. Hall, G. Iles, T. James, M. Komm, C. Laner, L. Lyons, A.-M. Magnan, S. Malik, A. Martelli, J. Nash[64], A. Nikitenko[7], V. Palladino, M. Pesaresi, A. Richards, A. Rose, E. Scott, C. Seez, A. Shtipliyski, G. Singh, M. Stoye, T. Strebler, S. Summers, A. Tapper, K. Uchida, T. Virdee[17], N. Wardle, D. Winterbottom, J. Wright, S.C. Zenz

Brunel University, Uxbridge, United Kingdom
J.E. Cole, P.R. Hobson, A. Khan, P. Kyberd, C.K. Mackay, A. Morton, I.D. Reid, L. Teodorescu, S. Zahid

Baylor University, Waco, USA
K. Call, J. Dittmann, K. Hatakeyama, H. Liu, C. Madrid, B. Mcmaster, N. Pastika, C. Smith

Catholic University of America, Washington, DC, USA
R. Bartek, A. Dominguez

The University of Alabama, Tuscaloosa, USA
A. Buccilli, S.I. Cooper, C. Henderson, P. Rumerio, C. West

Boston University, Boston, USA
D. Arcaro, T. Bose, D. Gastler, D. Rankin, C. Richardson, J. Rohlf, L. Sulak, D. Zou

Brown University, Providence, USA
G. Benelli, X. Coubez, D. Cutts, M. Hadley, J. Hakala, U. Heintz, J.M. Hogan[65], K.H.M. Kwok, E. Laird, G. Landsberg, J. Lee, Z. Mao, M. Narain, S. Sagir[66], R. Syarif, E. Usai, D. Yu

University of California, Davis, Davis, USA
R. Band, C. Brainerd, R. Breedon, D. Burns, M. Calderon De La Barca Sanchez, M. Chertok, J. Conway, R. Conway, P.T. Cox, R. Erbacher, C. Flores, G. Funk, W. Ko, O. Kukral, R. Lander,

M. Mulhearn, D. Pellett, J. Pilot, S. Shalhout, M. Shi, D. Stolp, D. Taylor, K. Tos, M. Tripathi, Z. Wang, F. Zhang

University of California, Los Angeles, USA
M. Bachtis, C. Bravo, R. Cousins, A. Dasgupta, A. Florent, J. Hauser, M. Ignatenko, N. Mccoll, S. Regnard, D. Saltzberg, C. Schnaible, V. Valuev

University of California, Riverside, Riverside, USA
E. Bouvier, K. Burt, R. Clare, J.W. Gary, S.M.A. Ghiasi Shirazi, G. Hanson, G. Karapostoli, E. Kennedy, F. Lacroix, O.R. Long, M. Olmedo Negrete, M.I. Paneva, W. Si, L. Wang, H. Wei, S. Wimpenny, B.R. Yates

University of California, San Diego, La Jolla, USA
J.G. Branson, P. Chang, S. Cittolin, M. Derdzinski, R. Gerosa, D. Gilbert, B. Hashemi, A. Holzner, D. Klein, G. Kole, V. Krutelyov, J. Letts, M. Masciovecchio, D. Olivito, S. Padhi, M. Pieri, M. Sani, V. Sharma, S. Simon, M. Tadel, A. Vartak, S. Wasserbaech[67], J. Wood, F. Würthwein, A. Yagil, G. Zevi Della Porta

University of California, Santa Barbara - Department of Physics, Santa Barbara, USA
N. Amin, R. Bhandari, J. Bradmiller-Feld, C. Campagnari, M. Citron, A. Dishaw, V. Dutta, M. Franco Sevilla, L. Gouskos, R. Heller, J. Incandela, A. Ovcharova, H. Qu, J. Richman, D. Stuart, I. Suarez, S. Wang, J. Yoo

California Institute of Technology, Pasadena, USA
D. Anderson, A. Bornheim, J.M. Lawhorn, H.B. Newman, T.Q. Nguyen, M. Spiropulu, J.R. Vlimant, R. Wilkinson, S. Xie, Z. Zhang, R.Y. Zhu

Carnegie Mellon University, Pittsburgh, USA
M.B. Andrews, T. Ferguson, T. Mudholkar, M. Paulini, M. Sun, I. Vorobiev, M. Weinberg

University of Colorado Boulder, Boulder, USA
J.P. Cumalat, W.T. Ford, F. Jensen, A. Johnson, M. Krohn, E. MacDonald, T. Mulholland, R. Patel, K. Stenson, K.A. Ulmer, S.R. Wagner

Cornell University, Ithaca, USA
J. Alexander, J. Chaves, Y. Cheng, J. Chu, A. Datta, K. Mcdermott, N. Mirman, J.R. Patterson, D. Quach, A. Rinkevicius, A. Ryd, L. Skinnari, L. Soffi, S.M. Tan, Z. Tao, J. Thom, J. Tucker, P. Wittich, M. Zientek

Fermi National Accelerator Laboratory, Batavia, USA
S. Abdullin, M. Albrow, M. Alyari, G. Apollinari, A. Apresyan, A. Apyan, S. Banerjee, L.A.T. Bauerdick, A. Beretvas, J. Berryhill, P.C. Bhat, G. Bolla[†], K. Burkett, J.N. Butler, A. Canepa, G.B. Cerati, H.W.K. Cheung, F. Chlebana, M. Cremonesi, J. Duarte, V.D. Elvira, J. Freeman, Z. Gecse, E. Gottschalk, L. Gray, D. Green, S. Grünendahl, O. Gutsche, J. Hanlon, R.M. Harris, S. Hasegawa, J. Hirschauer, Z. Hu, B. Jayatilaka, S. Jindariani, M. Johnson, U. Joshi, B. Klima, M.J. Kortelainen, B. Kreis, S. Lammel, D. Lincoln, R. Lipton, M. Liu, T. Liu, J. Lykken, K. Maeshima, J.M. Marraffino, D. Mason, P. McBride, P. Merkel, S. Mrenna, S. Nahn, V. O'Dell, K. Pedro, C. Pena, O. Prokofyev, G. Rakness, L. Ristori, A. Savoy-Navarro[68], B. Schneider, E. Sexton-Kennedy, A. Soha, W.J. Spalding, L. Spiegel, S. Stoynev, J. Strait, N. Strobbe, L. Taylor, S. Tkaczyk, N.V. Tran, L. Uplegger, E.W. Vaandering, C. Vernieri, M. Verzocchi, R. Vidal, M. Wang, H.A. Weber, A. Whitbeck

University of Florida, Gainesville, USA
D. Acosta, P. Avery, P. Bortignon, D. Bourilkov, A. Brinkerhoff, L. Cadamuro, A. Carnes,

M. Carver, D. Curry, R.D. Field, S.V. Gleyzer, B.M. Joshi, J. Konigsberg, A. Korytov, K.H. Lo, P. Ma, K. Matchev, H. Mei, G. Mitselmakher, D. Rosenzweig, K. Shi, D. Sperka, J. Wang, S. Wang, X. Zuo

Florida International University, Miami, USA
Y.R. Joshi, S. Linn

Florida State University, Tallahassee, USA
A. Ackert, T. Adams, A. Askew, S. Hagopian, V. Hagopian, K.F. Johnson, T. Kolberg, G. Martinez, T. Perry, H. Prosper, A. Saha, C. Schiber, R. Yohay

Florida Institute of Technology, Melbourne, USA
M.M. Baarmand, V. Bhopatkar, S. Colafranceschi, M. Hohlmann, D. Noonan, M. Rahmani, T. Roy, F. Yumiceva

University of Illinois at Chicago (UIC), Chicago, USA
M.R. Adams, L. Apanasevich, D. Berry, R.R. Betts, R. Cavanaugh, X. Chen, S. Dittmer, O. Evdokimov, C.E. Gerber, D.A. Hangal, D.J. Hofman, K. Jung, J. Kamin, C. Mills, I.D. Sandoval Gonzalez, M.B. Tonjes, H. Trauger, N. Varelas, H. Wang, X. Wang, Z. Wu, J. Zhang

The University of Iowa, Iowa City, USA
M. Alhusseini, B. Bilki[69], W. Clarida, K. Dilsiz[70], S. Durgut, R.P. Gandrajula, M. Haytmyradov, V. Khristenko, J.-P. Merlo, A. Mestvirishvili, A. Moeller, J. Nachtman, H. Ogul[71], Y. Onel, F. Ozok[72], A. Penzo, C. Snyder, E. Tiras, J. Wetzel

Johns Hopkins University, Baltimore, USA
B. Blumenfeld, A. Cocoros, N. Eminizer, D. Fehling, L. Feng, A.V. Gritsan, W.T. Hung, P. Maksimovic, J. Roskes, U. Sarica, M. Swartz, M. Xiao, C. You

The University of Kansas, Lawrence, USA
A. Al-bataineh, P. Baringer, A. Bean, S. Boren, J. Bowen, A. Bylinkin, J. Castle, S. Khalil, A. Kropivnitskaya, D. Majumder, W. Mcbrayer, M. Murray, C. Rogan, S. Sanders, E. Schmitz, J.D. Tapia Takaki, Q. Wang

Kansas State University, Manhattan, USA
S. Duric, A. Ivanov, K. Kaadze, D. Kim, Y. Maravin, D.R. Mendis, T. Mitchell, A. Modak, A. Mohammadi, L.K. Saini, N. Skhirtladze

Lawrence Livermore National Laboratory, Livermore, USA
F. Rebassoo, D. Wright

University of Maryland, College Park, USA
A. Baden, O. Baron, A. Belloni, S.C. Eno, Y. Feng, C. Ferraioli, N.J. Hadley, S. Jabeen, G.Y. Jeng, R.G. Kellogg, J. Kunkle, A.C. Mignerey, S. Nabili, F. Ricci-Tam, Y.H. Shin, A. Skuja, S.C. Tonwar, K. Wong

Massachusetts Institute of Technology, Cambridge, USA
D. Abercrombie, B. Allen, V. Azzolini, A. Baty, G. Bauer, R. Bi, S. Brandt, W. Busza, I.A. Cali, M. D'Alfonso, Z. Demiragli, G. Gomez Ceballos, M. Goncharov, P. Harris, D. Hsu, M. Hu, Y. Iiyama, G.M. Innocenti, M. Klute, D. Kovalskyi, Y.-J. Lee, P.D. Luckey, B. Maier, A.C. Marini, C. Mcginn, C. Mironov, S. Narayanan, X. Niu, C. Paus, C. Roland, G. Roland, G.S.F. Stephans, K. Sumorok, K. Tatar, D. Velicanu, J. Wang, T.W. Wang, B. Wyslouch, S. Zhaozhong

University of Minnesota, Minneapolis, USA
A.C. Benvenuti, R.M. Chatterjee, A. Evans, P. Hansen, S. Kalafut, Y. Kubota, Z. Lesko, J. Mans, N. Ruckstuhl, R. Rusack, J. Turkewitz, M.A. Wadud

University of Mississippi, Oxford, USA
J.G. Acosta, S. Oliveros

University of Nebraska-Lincoln, Lincoln, USA
E. Avdeeva, K. Bloom, D.R. Claes, C. Fangmeier, F. Golf, R. Gonzalez Suarez, R. Kamalieddin, I. Kravchenko, J. Monroy, J.E. Siado, G.R. Snow, B. Stieger

State University of New York at Buffalo, Buffalo, USA
A. Godshalk, C. Harrington, I. Iashvili, A. Kharchilava, C. Mclean, D. Nguyen, A. Parker, S. Rappoccio, B. Roozbahani

Northeastern University, Boston, USA
G. Alverson, E. Barberis, C. Freer, A. Hortiangtham, D.M. Morse, T. Orimoto, R. Teixeira De Lima, T. Wamorkar, B. Wang, A. Wisecarver, D. Wood

Northwestern University, Evanston, USA
S. Bhattacharya, O. Charaf, K.A. Hahn, N. Mucia, N. Odell, M.H. Schmitt, K. Sung, M. Trovato, M. Velasco

University of Notre Dame, Notre Dame, USA
R. Bucci, N. Dev, M. Hildreth, K. Hurtado Anampa, C. Jessop, D.J. Karmgard, N. Kellams, K. Lannon, W. Li, N. Loukas, N. Marinelli, F. Meng, C. Mueller, Y. Musienko[36], M. Planer, A. Reinsvold, R. Ruchti, P. Siddireddy, G. Smith, S. Taroni, M. Wayne, A. Wightman, M. Wolf, A. Woodard

The Ohio State University, Columbus, USA
J. Alimena, L. Antonelli, B. Bylsma, L.S. Durkin, S. Flowers, B. Francis, A. Hart, C. Hill, W. Ji, T.Y. Ling, W. Luo, B.L. Winer

Princeton University, Princeton, USA
S. Cooperstein, P. Elmer, J. Hardenbrook, S. Higginbotham, A. Kalogeropoulos, D. Lange, M.T. Lucchini, J. Luo, D. Marlow, K. Mei, I. Ojalvo, J. Olsen, C. Palmer, P. Piroué, J. Salfeld-Nebgen, D. Stickland, C. Tully

University of Puerto Rico, Mayaguez, USA
S. Malik, S. Norberg

Purdue University, West Lafayette, USA
A. Barker, V.E. Barnes, S. Das, L. Gutay, M. Jones, A.W. Jung, A. Khatiwada, B. Mahakud, D.H. Miller, N. Neumeister, C.C. Peng, S. Piperov, H. Qiu, J.F. Schulte, J. Sun, F. Wang, R. Xiao, W. Xie

Purdue University Northwest, Hammond, USA
T. Cheng, J. Dolen, N. Parashar

Rice University, Houston, USA
Z. Chen, K.M. Ecklund, S. Freed, F.J.M. Geurts, M. Kilpatrick, W. Li, B.P. Padley, J. Roberts, J. Rorie, W. Shi, Z. Tu, J. Zabel, A. Zhang

University of Rochester, Rochester, USA
A. Bodek, P. de Barbaro, R. Demina, Y.t. Duh, J.L. Dulemba, C. Fallon, T. Ferbel, M. Galanti, A. Garcia-Bellido, J. Han, O. Hindrichs, A. Khukhunaishvili, P. Tan, R. Taus

Rutgers, The State University of New Jersey, Piscataway, USA
A. Agapitos, J.P. Chou, Y. Gershtein, E. Halkiadakis, M. Heindl, E. Hughes, S. Kaplan, R. Kunnawalkam Elayavalli, S. Kyriacou, A. Lath, R. Montalvo, K. Nash, M. Osherson, H. Saka, S. Salur, S. Schnetzer, D. Sheffield, S. Somalwar, R. Stone, S. Thomas, P. Thomassen, M. Walker

University of Tennessee, Knoxville, USA
A.G. Delannoy, J. Heideman, G. Riley, S. Spanier

Texas A&M University, College Station, USA
O. Bouhali[73], A. Celik, M. Dalchenko, M. De Mattia, A. Delgado, S. Dildick, R. Eusebi, J. Gilmore, T. Huang, T. Kamon[74], S. Luo, R. Mueller, A. Perloff, L. Perniè, D. Rathjens, A. Safonov

Texas Tech University, Lubbock, USA
N. Akchurin, J. Damgov, F. De Guio, P.R. Dudero, S. Kunori, K. Lamichhane, S.W. Lee, T. Mengke, S. Muthumuni, T. Peltola, S. Undleeb, I. Volobouev, Z. Wang

Vanderbilt University, Nashville, USA
S. Greene, A. Gurrola, R. Janjam, W. Johns, C. Maguire, A. Melo, H. Ni, K. Padeken, J.D. Ruiz Alvarez, P. Sheldon, S. Tuo, J. Velkovska, M. Verweij, Q. Xu

University of Virginia, Charlottesville, USA
M.W. Arenton, P. Barria, B. Cox, R. Hirosky, M. Joyce, A. Ledovskoy, H. Li, C. Neu, T. Sinthuprasith, Y. Wang, E. Wolfe, F. Xia

Wayne State University, Detroit, USA
R. Harr, P.E. Karchin, N. Poudyal, J. Sturdy, P. Thapa, S. Zaleski

University of Wisconsin - Madison, Madison, WI, USA
M. Brodski, J. Buchanan, C. Caillol, D. Carlsmith, S. Dasu, L. Dodd, B. Gomber, M. Grothe, M. Herndon, A. Hervé, U. Hussain, P. Klabbers, A. Lanaro, K. Long, R. Loveless, T. Ruggles, A. Savin, V. Sharma, N. Smith, W.H. Smith, N. Woods

†: Deceased
1: Also at Vienna University of Technology, Vienna, Austria
2: Also at IRFU, CEA, Université Paris-Saclay, Gif-sur-Yvette, France
3: Also at Universidade Estadual de Campinas, Campinas, Brazil
4: Also at Federal University of Rio Grande do Sul, Porto Alegre, Brazil
5: Also at Université Libre de Bruxelles, Bruxelles, Belgium
6: Also at University of Chinese Academy of Sciences, Beijing, China
7: Also at Institute for Theoretical and Experimental Physics named by A.I. Alikhanov of NRC 'Kurchatov Institute', Moscow, Russia
8: Also at Joint Institute for Nuclear Research, Dubna, Russia
9: Also at Cairo University, Cairo, Egypt
10: Now at Helwan University, Cairo, Egypt
11: Also at Zewail City of Science and Technology, Zewail, Egypt
12: Also at Department of Physics, King Abdulaziz University, Jeddah, Saudi Arabia
13: Also at Université de Haute Alsace, Mulhouse, France
14: Also at Skobeltsyn Institute of Nuclear Physics, Lomonosov Moscow State University, Moscow, Russia
15: Also at Tbilisi State University, Tbilisi, Georgia
16: Also at Ilia State University, Tbilisi, Georgia
17: Also at CERN, European Organization for Nuclear Research, Geneva, Switzerland

18: Also at RWTH Aachen University, III. Physikalisches Institut A, Aachen, Germany

19: Also at University of Hamburg, Hamburg, Germany

20: Also at Brandenburg University of Technology, Cottbus, Germany

21: Also at MTA-ELTE Lendület CMS Particle and Nuclear Physics Group, Eötvös Loránd University, Budapest, Hungary, Budapest, Hungary

22: Also at Institute of Nuclear Research ATOMKI, Debrecen, Hungary

23: Also at Institute of Physics, University of Debrecen, Debrecen, Hungary, Debrecen, Hungary

24: Also at IIT Bhubaneswar, Bhubaneswar, India, Bhubaneswar, India

25: Also at Institute of Physics, Bhubaneswar, India

26: Also at Shoolini University, Solan, India

27: Also at University of Visva-Bharati, Santiniketan, India

28: Also at Isfahan University of Technology, Isfahan, Iran

29: Also at Plasma Physics Research Center, Science and Research Branch, Islamic Azad University, Tehran, Iran

30: Also at Università degli Studi di Siena, Siena, Italy

31: Also at Kyung Hee University, Department of Physics, Seoul, Korea

32: Also at International Islamic University of Malaysia, Kuala Lumpur, Malaysia

33: Also at Malaysian Nuclear Agency, MOSTI, Kajang, Malaysia

34: Also at Consejo Nacional de Ciencia y Tecnología, Mexico City, Mexico

35: Also at Warsaw University of Technology, Institute of Electronic Systems, Warsaw, Poland

36: Also at Institute for Nuclear Research, Moscow, Russia

37: Now at National Research Nuclear University 'Moscow Engineering Physics Institute' (MEPhI), Moscow, Russia

38: Also at St. Petersburg State Polytechnical University, St. Petersburg, Russia

39: Also at University of Florida, Gainesville, USA

40: Also at P.N. Lebedev Physical Institute, Moscow, Russia

41: Also at Budker Institute of Nuclear Physics, Novosibirsk, Russia

42: Also at Faculty of Physics, University of Belgrade, Belgrade, Serbia

43: Also at INFN Sezione di Pavia [a], Università di Pavia [b], Pavia, Italy, Pavia, Italy

44: Also at University of Belgrade: Faculty of Physics and VINCA Institute of Nuclear Sciences, Belgrade, Serbia

45: Also at Scuola Normale e Sezione dell'INFN, Pisa, Italy

46: Also at National and Kapodistrian University of Athens, Athens, Greece

47: Also at Riga Technical University, Riga, Latvia, Riga, Latvia

48: Also at Universität Zürich, Zurich, Switzerland

49: Also at Stefan Meyer Institute for Subatomic Physics, Vienna, Austria, Vienna, Austria

50: Also at Istanbul Aydin University, Istanbul, Turkey

51: Also at Mersin University, Mersin, Turkey

52: Also at Piri Reis University, Istanbul, Turkey

53: Also at Adiyaman University, Adiyaman, Turkey

54: Also at Gaziosmanpasa University, Tokat, Turkey

55: Also at Ozyegin University, Istanbul, Turkey

56: Also at Izmir Institute of Technology, Izmir, Turkey

57: Also at Marmara University, Istanbul, Turkey

58: Also at Kafkas University, Kars, Turkey

59: Also at Istanbul University, Istanbul, Turkey

60: Also at Istanbul Bilgi University, Istanbul, Turkey

61: Also at Hacettepe University, Ankara, Turkey

62: Also at Rutherford Appleton Laboratory, Didcot, United Kingdom

63: Also at School of Physics and Astronomy, University of Southampton, Southampton, United Kingdom

64: Also at Monash University, Faculty of Science, Clayton, Australia

65: Also at Bethel University, St. Paul, Minneapolis, USA, St. Paul, USA

66: Also at Karamanoğlu Mehmetbey University, Karaman, Turkey

67: Also at Utah Valley University, Orem, USA

68: Also at Purdue University, West Lafayette, USA

69: Also at Beykent University, Istanbul, Turkey, Istanbul, Turkey

70: Also at Bingol University, Bingol, Turkey

71: Also at Sinop University, Sinop, Turkey

72: Also at Mimar Sinan University, Istanbul, Istanbul, Turkey

73: Also at Texas A&M University at Qatar, Doha, Qatar

74: Also at Kyungpook National University, Daegu, Korea, Daegu, Korea